USAARL Report No. 94-49

The Effect of Binocular Overlap Mode on Contrast Thresholds Across the Field-of-View as a Function of Spatial and Temporal Frequency

By

Victor Klymenko
Robert W. Verona
John S. Martin
Howard H. Beasley

UES Incorporated

and

William E. McLean

Aircrew Health and Performance Division

September 1994

United States Army Aeromedical Research Laboratory
Fort Rucker, Alabama 36362-0577

Notice

Qualified requesters

Qualified requesters may obtain copies from the Defense Technical Information Center (DTIC), Cameron Station, Alexandria, Virginia 22314. Orders will be expedited if placed through the librarian or other person designated to request documents from DTIC.

Change of address

Organizations receiving reports from the U.S. Army Aeromedical Research Laboratory on automatic mailing lists should confirm correct address when corresponding about laboratory reports.

Disposition

Destroy this document when it is no longer needed. Do not return it to the originator.

Disclaimer

The views, opinions, and/or findings contained in this report are those of the author(s) and should not be construed as an official Department of the Army position, policy, or decision, unless so designated by other official documentation. Citation of trade names in this report does not constitute an official Department of the Army endorsement or approval of the use of such commercial items.

Reviewed:

RICHARD R. LEVINE
LTC, MS
Director, Aircrew Health and Performance Division

ROGER W. WILEY, O.D., Ph.D.
Chairman, Scientific
Review Committee

Released for publication:

DENNIS F. SHANAHAN
Colonel, MC, SFS
Commanding

Unclassified
SECURITY CLASSIFICATION OF THIS PAGE

REPORT DOCUMENTATION PAGE

Form Approved OMB No. 0704-0188

1a. REPORT SECURITY CLASSIFICATION Unclassified	1b. RESTRICTIVE MARKINGS
2a. SECURITY CLASSIFICATION AUTHORITY	3. DISTRIBUTION/AVAILABILITY OF REPORT Approved for public release; distribution unlimited
2b. DECLASSIFICATION/DOWNGRADING SCHEDULE	
4. PERFORMING ORGANIZATION REPORT NUMBER(S) USAARL Report No. 94-49	5. MONITORING ORGANIZATION REPORT NUMBER(S)
6a. NAME OF PERFORMING ORGANIZATION U.S. Army Aeromedical Research Laboratory 6b. OFFICE SYMBOL (If applicable) SGRD-UAS-VS	7a. NAME OF MONITORING ORGANIZATION U.S. Army Medical Research, Development, Acquisition and Logistics Command(Provisional)
6c. ADDRESS (City, State, and ZIP Code) P.O. Box 620577 Fort Rucker, AL 36362-0577	7b. ADDRESS (City, State, and ZIP Code) Fort Detrick Frederick, MD 21702-5012
8a. NAME OF FUNDING/SPONSORING ORGANIZATION 8b. OFFICE SYMBOL (If applicable)	9. PROCUREMENT INSTRUMENT IDENTIFICATION NUMBER
8c. ADDRESS (City, State, and ZIP Code)	10. SOURCE OF FUNDING NUMBERS PROGRAM ELEMENT NO. 0602787A; PROJECT NO. 3E1672 787A879; TASK NO. BG; WORK UNIT ACCESSION NO. 164

11. TITLE (Include Security Classification)
(U) The Effect of Binocular Overlap Mode on Contrast Thresholds Across the Field-of-View as a Function of Spatial and Temporal Frequency

12. PERSONAL AUTHOR(S)
Victor Klymenko, Robert W. Verona, John S. Martin, Howard H. Beasley, William E. McLean

13a. TYPE OF REPORT	13b. TIME COVERED	14. DATE OF REPORT (Year, Month, Day)	15. PAGE COUNT
Final	FROM _____ TO _____	1994 September	59

16. SUPPLEMENTARY NOTATION

17. COSATI CODES			18. SUBJECT TERMS (Continue on reverse if necessary and identify by block number)
FIELD	GROUP	SUB-GROUP	convergent FOV, divergent FOV, partial binocular overlap, full binocular overlap, luning, binocular threshold, spatial frequency, temporal frequency
14	23		
04	02		

19. ABSTRACT (Continue on reverse if necessary and identify by block number)

Two partial binocular overlap display modes, the convergent display mode and the divergent display mode, have been proposed as alternatives to the full binocular overlap display mode in helmet-mounted displays. In the full binocular overlap display mode, the entire field-of-view (FOV) is binocular. The partial overlap display modes increase the FOV by reducing the size of the binocular overlap region and introducing two flanking monocular regions. Visual sensitivity is known to be lower in monocular regions. Another consequence of the partial binocular overlap display mode is a perceptual effect known as luning, which is a subjective darkening in the monocular regions near the binocular overlap border due to dichoptic stimulation. Luning has been shown to be more severe in the divergent display mode compared to the convergent display mode. The purpose of our study was to investigate the effect of these display modes on visual sensitivity across the FOV. It was hypothesized that visual thresholds would be highest in the divergent mode, where luning was most severe, and lowest in the full overlap mode, where there was no dichoptic stimulation. We measured the visual threshold to probe targets across the FOV for (1) the full overlap, (2) the convergent mode, and (3) the divergent mode.
Continued

20. DISTRIBUTION/AVAILABILITY OF ABSTRACT	21. ABSTRACT SECURITY CLASSIFICATION
☒ UNCLASSIFIED/UNLIMITED ☐ SAME AS RPT. ☐ DTIC USERS	Unclassified
22a. NAME OF RESPONSIBLE INDIVIDUAL Chief, Science Support Center	22b. TELEPHONE (Include Area Code) (205) 255-6907 22c. OFFICE SYMBOL SGRD-UAX-SI

DD Form 1473, JUN 86 *Previous editions are obsolete.*

19. Abstract Continued

The experimental conditions included four types of position in the FOV: monocular and binocular, each of which could be either adjacent or nonadjacent to the binocular overlap border. All combinations of four spatial (8.48, 4.24, 2.12, and 1.06 cycles per degree) and four temporal frequency (0, 3.75, 7.5, and 15 Hertz) probe targets were tested at each of the four locations. We found, as expected, that the probe target thresholds for monocular stimuli in the partial overlap display modes were higher than the thresholds for the binocular stimuli at the corresponding positions in the full overlap display mode. We also found, in general, that thresholds were higher in the divergent than in the convergent display mode and that this difference was greatest near the binocular overlap border. Overall these differences were more pronounced for the highest spatial frequencies. These results are discussed in terms of the visual interpretations of display modes based on visual geometric constraints.

Table of contents

Page

Introduction 3

Background concepts 3
Luning and fragmentation 4
Binocular and monocular contrast thresholds 6
Purpose of study 7

Method 8

Subjects 8
Equipment 8
Stimuli 11
Binocular overlap display modes 11
Fusion locks and fusion stimulus pattern 14
Optical convergence 14
Probe stimuli 15
Probe positions 17
Design 18
Procedure 20
Data analysis 21

Results and discussion 22

Contrast thresholds 22
Summary of results 24
Discussion 24

References 29

Appendix A Eye exam data sheet 32
Appendix B Manufacturers' list 33
Appendix C Results tables 34
Appendix D Results figures 43

List of illustrations

Figure		Page
1.	Partial binocular overlap display mode	5
2.	Perspective view of optical table configuration, consisting of the monitor, eight mirrors, and a pair of binoculars	9
3.	Top view of optical table configuration	10
4.	Dimensions of elliptical monocular fields and fusion stimulus pattern	12
5.	Display modes	13
6.	Spatial modulation of probe stimuli	16
7.	Temporal modulation of probe stimuli	17
8.	The four probe positions	18
9.	Experimental displays	19
10.	Visual geometric interpretation of the divergent display mode	26
11.	Visual geometric interpretation of the convergent display mode	27
12.	Retinal projection of the fixation point and off-fixation points in near space and far space	28

Introduction

Small fields-of-view (FOV) are detrimental to the visual tasks required of military pilots (Kenyon and Kneller, 1993; Osgood and Wells, 1991; Wells, Venturino, and Osgood, 1989; Wolpert, 1990). In order to increase the extent of the visual world available to U.S. Army helicopter pilots using helmet mounted displays (HMD) without incurring increases in size, weight, or loses in central resolution, an unusual method of display---partial binocular overlap---has been proposed. Two flanking monocular regions and a central binocular overlap region constitute the FOV in partial binocular overlap displays. Increasing the FOV by this method has been the cause of some concern (see Alam, Zheng, Iftekharuddin, and Karim, 1992; Edgar, Carr, Williams, and Clark, 1991; Kruk and Longridge, 1984; Landau, 1990; Moffitt, 1989; see Moffitt, 1991, and Moffitt and Melzer, 1991, for a tutorial description). One detrimental consequence of the partial binocular overlap display mode is a perceptual effect known as luning, which is a subjective darkening in the monocular regions of the FOV (Moffitt, 1989; Klymenko et al., 1994b). Luning may also be experienced as a visual fragmentation of the FOV into three distinct regions (Klymenko et al., 1994a). Our concern here is the effect on target detection in the FOV of partial binocular overlap displays. The purpose of this study was to investigate the effects of partial binocular overlap displays on visual sensitivity across the FOV. First, we define a few concepts to clarify the ambiguity of the literatures on vision and display systems (see Farrell and Booth, 1984).

Background concepts

In the visual displays described here, **background** is the black region surrounding the **visual fields**, which are the intentionally stimulated visual areas available to each eye. Access to the visual world is assumed to occur only through these artificial visual fields. **Field-of-view** (FOV) refers to the total extent of the visual world that is seen in an HMD when both eyes are open. It includes what is seen by both eyes together as well as by each eye alone. The portion of the visual world that one eye sees is referred to as its **monocular field**. The portion of the visual world seen by both eyes together is referred to as the **binocular overlap region**, and the portion of the FOV that only one eye sees is a **monocular region**. Thus, the FOV may consist of both a binocular overlap region and a monocular region for each eye.

A monocular field may consist of two areas, a monocular region seen exclusively by one eye and the binocular overlap region which can be seen by both eyes. Separating these two areas is the binocularly defined **binocular overlap border**. The term **dichoptic** refers to the case where there is a simultaneous but dissimilar stimulation to the two eyes; thus, a monocular region and its corresponding region in the other eye, as well as the binocular border, are dichoptic. The binocular attainment of **singleness of vision** results from the **binocular fusion** of monocular stimuli in corresponding retinal regions of each eye. **Diplopia**, or double vision, results when corresponding monocular stimuli fail to be fused.

When the two eyes are presented with exactly the same portion of the visual world, the viewing situation is referred to as the **full binocular overlap display mode**. In this case, the FOV consists solely of a binocular overlap region, in which the two monocular fields are coincident and there are no monocular regions. The **partial binocular overlap display mode** occurs when each of the two eyes sees a portion of the visual world in common---the binocular overlap region---and, in addition, each eye sees an exclusive portion of the visual world in the monocular region.

A word of caution on the difference in the use of terms in the applied display literature compared to the basic vision literature is that the display literature often refers to the effective or intended visual experience rather than the normal or potential experience. For example, in the display literature, the terms "field-of-view" and "monocular fields" refer to the intentionally induced, or effective field-of-view and monocular fields. This usage could have the unintentional effect of ignoring factors outside the display definitions, such as, for example, the low luminance background surrounding the effective FOV. With this in mind, unless indicated otherwise, we follow the display literature terms defined here.

Partial binocular overlap displays contain binocular overlap borders, which in terms of the FOV, separate the binocular overlap region and the monocular regions. In terms of the monocular fields, these borders separate the portion exclusively seen by one eye from the portion seen in common with the other eye. In normal unencumbered vision, the binocular overlap borders, dividing the natural FOV, are not experienced per se (see Gibson, 1979, for an authoritative discussion), and are only cognitively identified and located with considerable attentional effort. However, in artificial viewing situations such as HMDs where the monocular fields are smaller than in natural viewing, these borders are accompanied by a perceptual effect that in the display literature has come to be known as luning (see CAE Electronics, 1984; Moffitt, 1989).

Luning and fragmentation

Luning is a visual perception characterized by a subjective darkening of the visual field in the monocular regions of partial binocular overlap displays. Having first been documented with binocular HMDs used in simulators (CAE Electronics, 1984), luning was so named because of the crescent shapes of the darkened monocular regions adjacent to the circular binocular overlap region (Moffitt, 1989; Melzer and Moffitt, 1989; Klymenko et al., 1994b). It is most pronounced near the binocular overlap border separating the monocular and binocular regions, gradually fading with increasing distance from the border. The magnitude of luning can fluctuate over time, and it appears not to be strongly under attentional control (see Figure 1). Under some conditions, luning may be experienced as **fragmentation** of the FOV into three phenomenally distinct regions, where the central

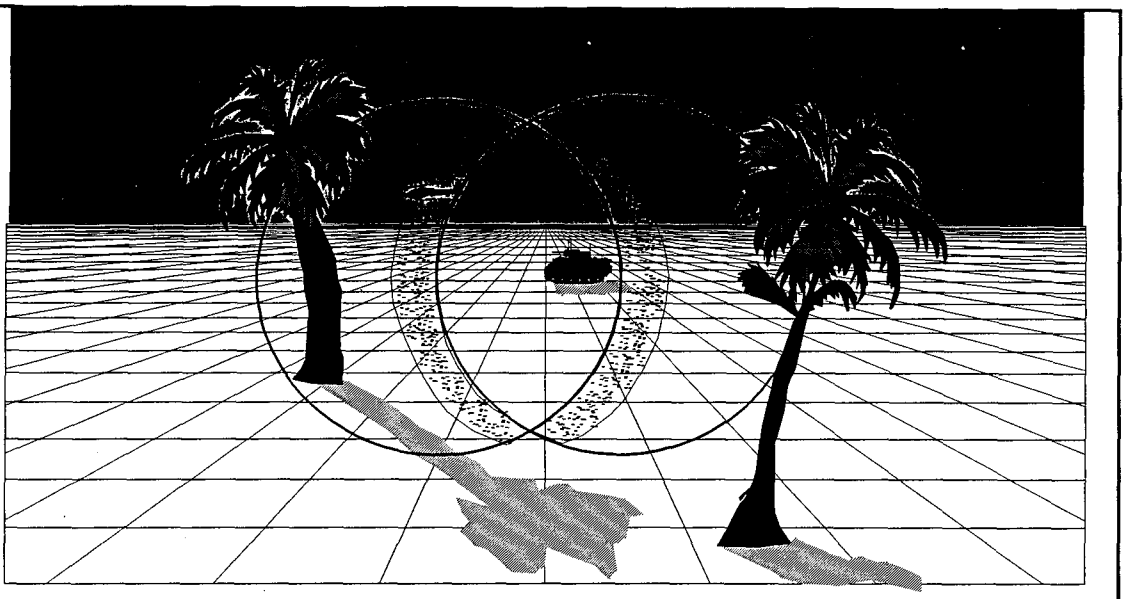

Figure 1. *Partial binocular overlap display mode. A helicopter pilot's view of the visual world using a helmet mounted display in the partial binocular overlap display mode, where each eye sees a circular monocular field against a black background. The armored personnel carrier is in the* ***binocular overlap region.*** *Flanking this region are the two monocular regions. A helicopter is in the monocular region. If the right eye views the circular field on the right, the effective* ***field-of-view*** *is in the* ***divergent*** *display mode; if the right eye instead views the left circular field, the mode is* ***convergent.*** *Separating the central binocular region and flanking monocular regions are the* ***binocular overlap borders.*** *Under some conditions, these borders become phenomenally apparent, where the field-of-view no longer appears to be a unitary and continuously clear view of the visual world.*

Luning *refers to the subjective darkening which can occur in the flanking monocular regions near the binocular overlap borders.* ***Fragmentation*** *is the appearance of the field-of-view as three phenomenally distinct regions. These deleterious effects are caused by strong* ***dichoptic*** *stimulation from the dark background and monocular field borders in each eye with the corresponding locations within the monocular field of the contralateral eye.*

The purpose of the current study was to investigate how visual sensitivity across the field-of-view is affected by the ***convergent*** *display mode, the* ***divergent*** *display mode and the* ***full overlap*** *display mode. In the full overlap mode each eye sees the same monocular image.*

binocular overlap region appears to be different than the two monocular side regions (Klymenko et al., 1994a). The monocular regions may appear to lie in a different depth plane, to be darker and less substantial and less stable than the binocular overlap region, as well as to fluctuate in appearance over time.

Luning and fragmentation may be due to binocular rivalry and suppression. **Binocular rivalry** refers to the phenomenal alterations in appearance of a binocular stimulus, which is dichoptic; in our case, the monocular regions in the partial binocular overlap display modes. Over time, one and then the alternative dichoptic stimuli successfully may compete and dominate awareness. **Suppression** refers to the phenomenal disappearance of one eye's input due to **monocular dominance** by the other eye. Partial suppression refers to the partial disappearance of one eye's input. In the partial binocular overlap display mode, each eye's monocular region is the result of dichoptic competition between a portion of its monocular field and the dark background of the other eye. If the background is completely suppressed, the FOV looks natural, where the binocular and monocular regions both are seen as one continuous visual world. If one eye's monocular region is partially suppressed by the dark background of the other eye, then this dark background will appear in the monocular regions of the first eye with the greatest darkening---luning---occurring near the binocular overlap border. With a sufficiently small display size, this luning is experienced as a fragmentation of the FOV into three distinct visual regions where the two flanking monocular regions appear separate from and different than the central binocular overlap region. The monocular region is the binocular result of the dichoptic combination of the monocular field of one eye and the background of the contralateral eye. Visual dominance by the eye contributing the monocular field to the monocular region results in a unitary or stable appearance, while dominance by the eye contributing the background results in luning and fragmentation. We refer to the eye contributing the monocular field to the monocular region as the **informational** eye, and the eye contributing the background and border as the **non-informational** eye.

In the monocular regions of partial binocular overlap displays, both the dichoptic differences in luminance, and the presence of the luminance transition at the monocular field border in the noninformational eye likely both affect luning and fragmentation. Binocular rivalry and the interocular inhibitory process of suppression due to rivalry likely are the causes of luning and fragmentation. Elsewhere, we have shown that in partial binocular overlap displays, luning and fragmentation are more severe in the divergent compared to the convergent display mode (Klymenko et al., 1994a, 1994b).

Binocular and monocular contrast thresholds

In addition to the advantages resulting from stereopsis per se, binocular vision is superior to monocular vision in a number of ways including form recognition, reaction time to stimulus onset and visual detection threshold. This superiority generally occurs under the constraint of synchronous and retinally corresponding stimulation in the two eyes (Arditti, 1986). Much of the literature has been focused on determining the degree to which binocular

superiority is due to neural as opposed to probability summation (see Arditti, 1986; and Boff and Lincoln, 1988, for reviews). Contrast threshold is most relevant to perceptual tasks such as object recognition and detection. Contrast threshold is the degree of contrast in an image required to perform a perceptual task. It is often reported in terms of its reciprocal, which is contrast sensitivity. A number of studies have demonstrated the superiority of binocular versus monocular contrast sensitivity, with the ratio of binocular enhancement often reported to be around 1.4 (Campbell and Green, 1965). In the partial binocular overlap displays, the total FOV is increased at the expense of the size of the binocular overlap region. Thus, because of the lower sensitivity of stimuli in monocular regions, the FOV may be increased at the expense of sensitivity. Of interest is, how much of a difference in sensitivity is there? Also, there may be a further difference due to the mode of the partial binocular overlap display. That is, is there a difference between the convergent and the divergent display modes, and does this correspond to the luning and fragmentation effects? Also, since edges are strong dichoptic competitors that pull neighboring regions into the binocular percept (Kaufman, 1963), does distance to the binocular overlap edge affect threshold?

Purpose of study

The current investigation was designed to determine how partial overlap display modes affect target contrast thresholds required for identification. We measured the contrast threshold to probe targets at various positions across the FOV to determine first, how distance to the binocular overlap border affects targets in the two partial overlap display modes; second, how monocular and binocular presentation of the target affects threshold; and third, how partial overlap display modes compare to the full overlap display mode. We tested probe targets sampled from a range of spatial frequencies and temporal frequencies (1.06, 2.12, 4.24 and 8.48 cycles per degree [cpd]), and (0, 3.75, 7.5 and 15 Hertz [Hz]), respectively. The rationale for using these frequencies follows. The spatial frequency contrast sensitivity curve normally peaks at an intermediate frequency (2-5 cpd) with a drop off at lower and higher frequencies (Campbell and Robson, 1968). Thus, we employed low, intermediate, and high spatial frequencies to sample the range of spatial frequencies. Due to the central importance of motion perception to piloting (e.g., Kenyon and Kneller, 1993; Wolpert, 1990), we also included a range of temporal frequencies to probe the range of motion sensitivity. Motion mechanisms are thought to peak around 6 to 8 Hz (see Nakayama, 1985, for a review). Thus, we employed low, intermediate, and high temporal frequencies as well as stationary targets, zero Hz, to sample the range of human temporal sensitivity. Sensitivity is dependent on both spatial and temporal frequency (see Plant, 1991, for a review), so we tested each spatial and temporal frequency combination.

Our main purpose was to determine the effect on target perception of presenting the FOV under the three display modes. We did this by measuring the contrast thresholds needed to identify targets for each of the three display modes for a range of spatial and temporal frequency probe targets at a number of positions across the FOV. In summary, the purpose was to determine how visual sensitivity across the FOV is affected when a pilot's FOV is

increased by changing from a full binocular overlap display mode to one of two versions of a partial binocular overlap display mode. In addition, we determined the differences between the convergent and divergent partial overlap display modes, and the effect on sensitivity of the proximity of the binocular overlap border to the target.

Method

Subjects

Thirty-one Army aviator student volunteers, 30 males and 1 female, took part in the experiment. Army aviator students are a population which has undergone rigorous vision screening. All had 20/20 unaided or better Snellen acuity. Each subject's vision was checked before the experiment using the standard Armed Forces Vision Tester. Also, the accommodative/convergence relationship and the interpupillary distance (IPD) of each subject were measured and recorded. A copy of the exam data sheet is provided in Appendix A. Average age was 25 (SD=2.7), ranging from 19 to 30.

Equipment

The equipment consisted of three major components: A Hewlett-Packard HP-98731 Turbo-SRX computer graphics workstation used to generate the visual stimuli; a custom optical table configuration used to optically direct the visual stimuli from the workstation monitor to a pair of Adlerblick viewing binoculars (Edmund Scientific); and a subject booth.[1] The booth was a light-proof enclosure behind the binoculars, in which the subject viewed the stimuli via the binoculars and responded with an HP response keypad, or "button box."

The HP-98731 Turbo-SRX computer graphics workstation consisted of a 19-inch color Trinitron monitor (1280 x 1024 pixels) for presenting visual stimuli, and a computer for generating the stimuli, recording the responses, and analyzing the data. Connected to the workstation were the experimenter's terminal to allow the experimenter to run the experimental programs and monitor the progress of each test session; an external monitor tied to the HP computer via a scan converter to allow the experimenter to unobtrusively view the experimental stimuli presented to the subject; and the button box, a 32-button keypad to allow the subject to respond to the visual stimulus presentations.

The optical table configuration (Figures 2 and 3) consisted of a 4 foot x 6 foot optical table, with the workstation monitor mounted at one wide end of the table, and eight front-

[1] See Manufacturers' list in Appendix B.

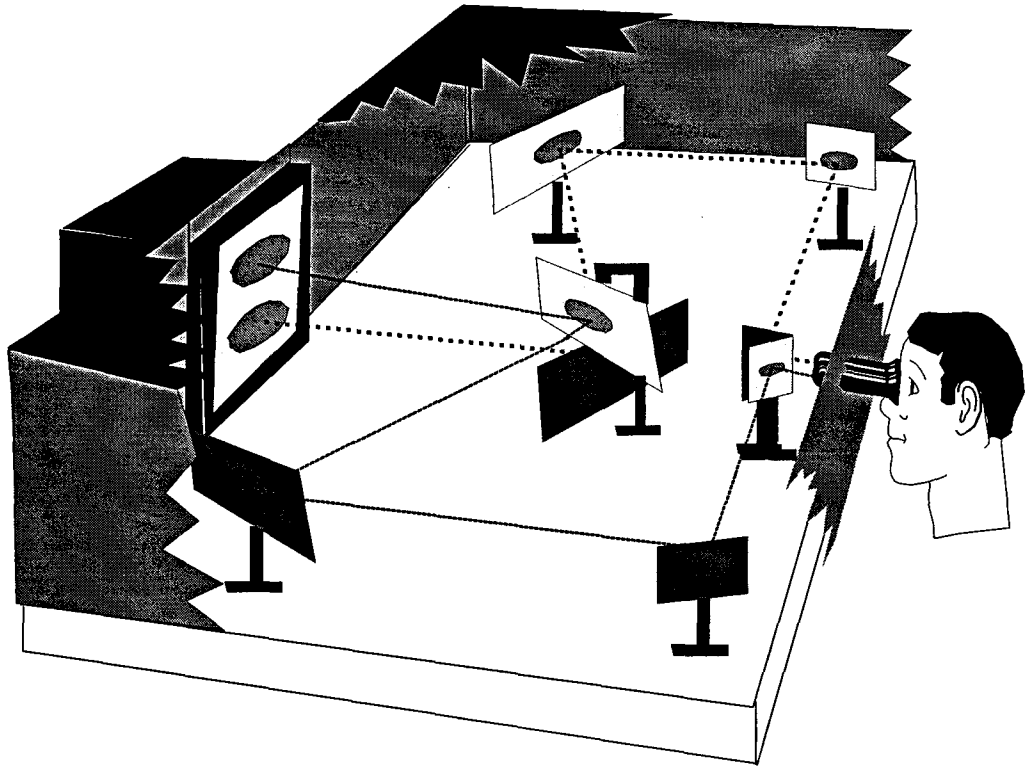

Figure 2. *Perspective view of the optical table configuration, consisting of the monitor, eight mirrors, and a pair of binoculars (not to scale). The image from the top half of the monitor was directed to the left eye and the image from the bottom half was directed to the right eye. Additional equipment, not shown, included a light baffle in front of the monitor between the two optical paths, focusing lenses attached to the binoculars, and filter holders in front of the binoculars.*

surfaced mirrors mounted on the table to direct the visual image--the optical train--to a pair of viewing binoculars mounted on the other wide end of the table. The purpose of the eight mirrors was to allow the independent presentation of two channels, one to each ocular of the binoculars, from the same monitor. Through the binoculars, the image on the top half of the monitor was seen by the left eye and the image on the bottom half of the monitor was seen by the right eye. The 7x50 binoculars were mounted onto a fixture which allowed IPD to be precisely adjusted for each subject. Affixed on the front of the binoculars were auxiliary focusing lenses to focus the magnified image for the optical train viewing distance. A light baffle in front of the monitor between the two optical paths was positioned to prevent cross talk between the two image channels. Filter holders in front of the binoculars allowed the placement of neutral density optical filters. The two mirrors, depicted L4 and R4 in Figure 3, mounted directly in front of the binoculars, were movable to allow adjustments corresponding

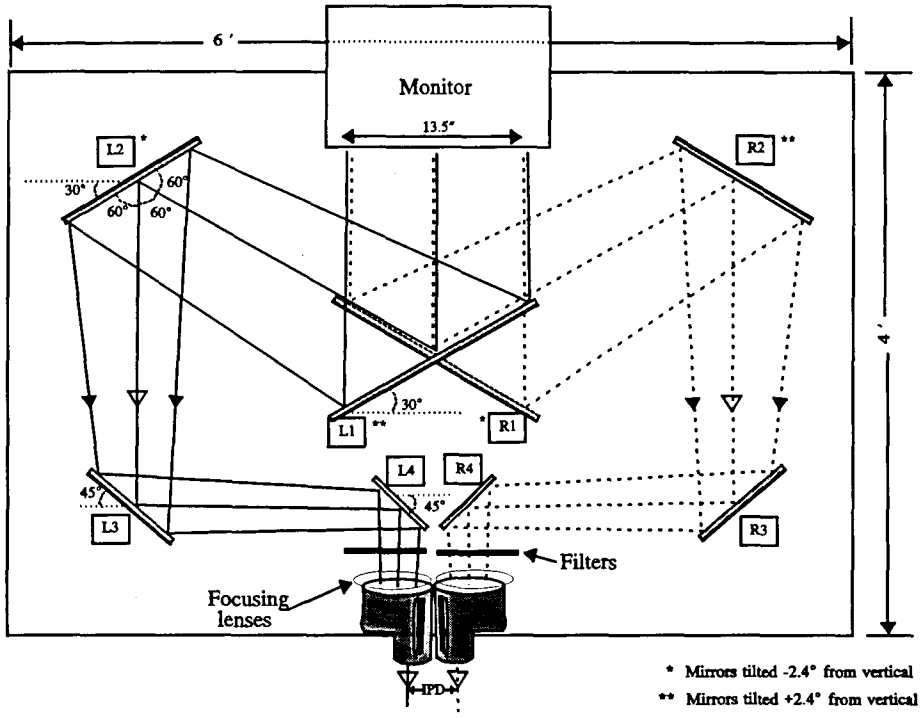

Figure 3. *Top view of the optical table configuration. The image from the top half of the monitor (solid rays) is reflected down from mirror L1 to L2, and then parallel to the surface of the table, from mirrors L2 to L3 to L4 to the left ocular of the binoculars. Similarly for the right channel, the image from the bottom half of the monitor (dashed rays) was reflected up from mirror R1 to R2, and then parallel to the surface of the table from mirrors R2 to R3 to R4 to the right ocular of the binoculars. The binoculars and movable mirrors L4 and R4 are set to correspond to each individual subject's interpupillary distance.*

to the IPD settings of the binoculars. These adjustments to the distance between L4 and L3, and R4 and R3, ensured a properly centered image for each IPD setting.

The optical table configuration was designed to allow the horizontal extent of the monitor (1280 pixels) to match the horizontal visual extent (diameter) of each ocular of the binoculars. The resulting images seen through each ocular were 50 degrees of visual angle corresponding to 1280 pixels, or 25.6 pixels per degree of visual angle. The temporal resolution, or frame rate of the monitor, was 60 Hz noninterlaced. The 7x50 Adlerblick binoculars have a vertex distance of 27 mm, and an exit pupil diameter of 7.14 mm.

The convex cylindrical surface of the monitor (approximately 1.5 meter radius of curvature) resulted in a focal distance disparity for the center and edges of the display seen through the binoculars. The focusing difference between the center and extreme edge of the image on the monitor, measured with a diopterscope, was approximately 0.75 diopters. To ensure a clear image for the test stimuli within the field-of-view used, the binoculars were focused with the diopterscope to -0.50 diopters (2 meters) for the center of the display. This ensured that subjects, all younger than 30 years of age, could easily accommodate to any part of the FOV.

Covering the optical table and the subject booth was a metal frame covered by black cloth to prevent light leakage and to protect the optical table components. The subject booth was a light-proof enclosure in which the subject was seated at an adjustable chin rest affixed in front of the binoculars. Except for the stimuli viewed through the binoculars, the subject was in darkness. Mounted on the end of the optical table in front of the subject was a call switch which rang a buzzer. Mounted within easy access of the subject was the button box used to register the subject's responses. Above the subject was an adjustable air vent connected to the air conditioning to allow the subject control of the temperature in the subject booth.

Stimuli

There were three binocular overlap display modes---the convergent partial overlap display mode, the divergent partial overlap display mode, and the full overlap display mode. These are described in the following section. Visual thresholds to probe stimuli in the FOV were measured for each of the three display modes to determine how display mode affects visual sensitivity. This was done at a number of positions across the FOV for probes of various spatial and temporal frequencies as described below.

Binocular overlap display modes

The visual field of each eye's view through the binoculars consisted of a gray ellipse whose dimensions were 30 degrees of visual angle (768 pixels horizontal diameter) x 16 degrees of visual angle (410 pixels vertical diameter) against a black background. In each circular (50 degrees diameter) ocular view through the binoculars, the gray ellipses for each display mode were located centrally in the vertical dimension and horizontally located as described below. These ellipses represented each eye's monocular visual field; the horizontal relationship between them defined the display mode (see Figure 4).

If the ellipses each were located centrally so that there was full binocular overlap of each of the monocular fields, the total horizontal FOV was 30 degrees, the same as each monocular field. This was designated the **full overlap display mode** (see Figure 5).

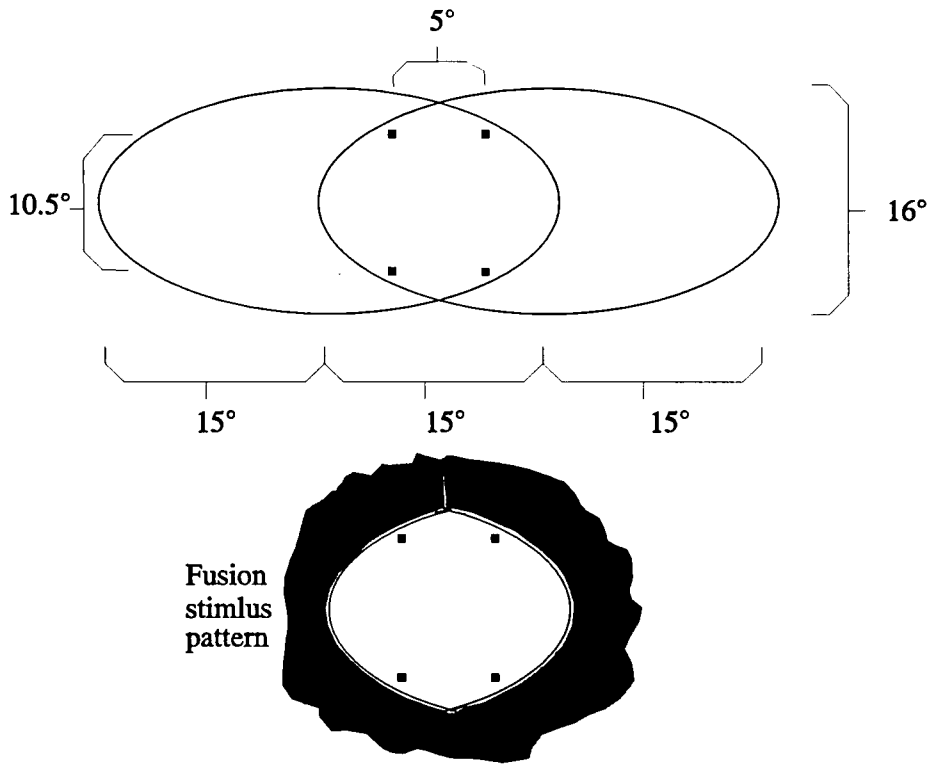

Figure 4. *Dimensions of elliptical monocular fields and fusion stimulus pattern. The visual dimensions in degrees of visual angle are given to the right and below the overlapping monocular ellipses. The distances between fusion locks are given above and to the left. The fusion stimulus pattern, in which the same image was presented to both eyes, is shown below the ellipses. This pattern consisted of the fusion locks and the binocular overlap region.*

If the elliptical fields for the right and left eyes were moved, respectively, 7.5 degrees to the right and left of the full overlap position, the monocular fields remained the same in extent, but the total FOV increased to 45 degrees. Both eyes now saw a smaller central binocular overlap region of 15 degrees, while each individual eye saw a flanking monocular region of 15 degrees. Because the right eye saw the flanking monocular region to the right of the binocular region, and the left eye saw a flanking monocular region to the left of the binocular region, the display mode was **divergent**, which, except for the sizes of the visual regions, is what is seen in normal human vision.

Conversely, if the elliptical field for the right and left eyes were, respectively, moved 7.5 degrees to the left and right of the full overlap position, then the display mode was **convergent**. Now both eyes again saw the same smaller central binocular region of 15 degrees, the total FOV again was increased to 45 degrees, but this time the right eye's

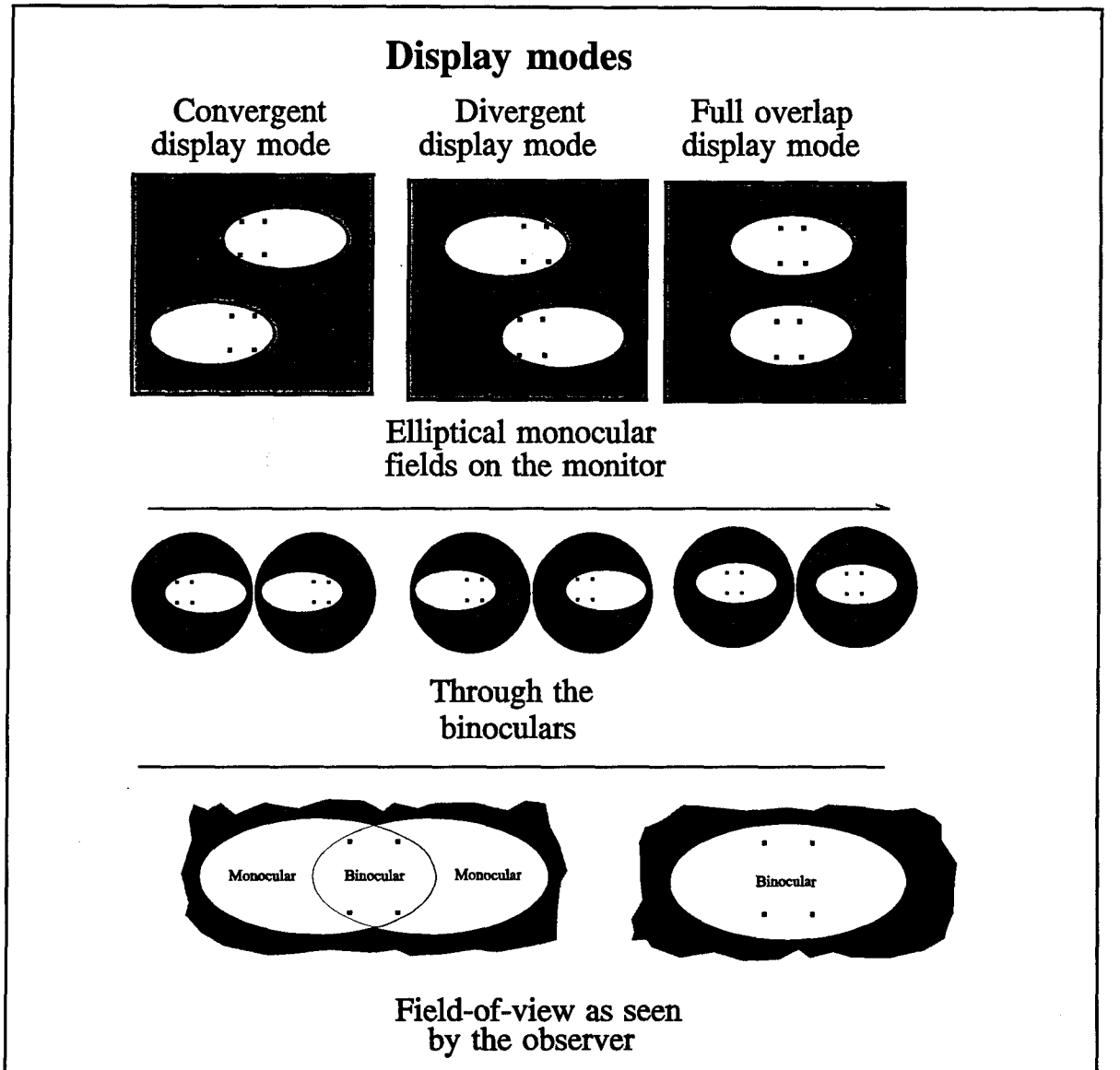

Figure 5. *Display modes. The **top panel** shows the elliptical monocular fields on the monitor for each of the three display modes. The **middle panel** shows the images of the monocular fields through the binoculars for each display mode. The **bottom panel** show the field-of-view as seen by the observer when the monocular images are fused properly. The image on the right corresponds to the full overlap display mode and the image on the left corresponds to either the convergent or the divergent display modes. The small black squares are the fusion locks.*

flanking monocular region was to the left of the binocular region, while the left eye's flanking monocular region was to the right of the binocular region. (This can be simulated by looking through an aperture.) The luminance through the binoculars of the elliptical fields was approximately 2.0 footlamberts against a dark background of 0.02 footlamberts.

Fusion locks and fusion stimulus pattern

Simply shifting the images as described above is no guarantee that subjects will binocularly fuse the images. Subjects need similar stimuli common to both eyes to prevent disjunctive eye movements in order to binocularly fuse images properly and to avoid image slippage, which leads to the binocular overlap of inappropriate regions of the two monocular images. To ensure "binocular locking" of the appropriate areas of the monocular fields, four "fusion locks" always were present in each eye's image in the binocular region at the appropriate locations in each image. These are the small black rectangles (2 pixel horizontal x 8 pixel vertical) located as shown in the ellipses in Figure 4. The fusion locks were located symmetrically above and below the long axis of the ellipses, and to the right and left of the center of the fused overlap region as shown in Figure 4. Throughout the experiment, each subject had access, via the button box, to a fusion stimulus pattern in order to return fusion in the event it was lost. This stimulus consisted of an identical image for each eye (see bottom of Figure 4). It consisted of the four fusion locks and the binocular overlap region of the elliptical monocular fields in the partial overlap display modes. The luminance of this pattern was 2.0 footlamberts against the black background. A subject knew to call this pattern if diplopia was experienced, or if more than four fusion locks were seen, indicating that fusion was not occurring properly.

Optical convergence

Optical convergence and accommodation were both set for 2 meters at the center of the display. Optical convergence here refers to the angle between the optical axes of the eyes and should not be confused with the convergent display mode. Since the centers of both the right and left eye images were focused to 2 meters (-0.50 diopters) through the binoculars, the right and left images also were positioned so that the eyes converged to 2 meters. This was for an "average" subject with an IPD separation of 64 mm. Convergence was induced by shifting each eye's image on the monitor 0.92 degrees of visual angle (22 pixels) in the nasal direction. The range of IPDs for the 31 subjects was 57 mm to 69 mm, with a mean of 64 mm (SD=2.7). For this group of subjects, the fixed convergence induced convergence demands of from 1.78 meters (for a 57 mm IPD) to 2.15 meters (for a 69 mm IPD). This is less than 0.35 prism diopters (3.5 milliradians) of residual fusional convergence or divergence required for an image located at 2 meters.

Probe stimuli

The probe stimuli consisted of spatially and temporally modulated patterns located within the monocular visual fields. The luminance of the probes were modulated about 2.0 footlamberts, which was the luminance of the gray elliptical monocular fields.

Spatially, the probe stimuli were circular patches generated as follows: There were four cycles of a sine wave, which always began, ended, and was centered on a zero crossing (set to 2.0 footlamberts). The phase of the sine wave was either 0 or 180 degrees. The orientation of the sine wave was either 45 degrees to the left or 45 degrees to the right of vertical. This sine wave was multiplied by a half cycle of a circularly symmetric cosine envelope of one-fourth the sine wave spatial frequency, where the center of the circular envelope was the peak of the cosine and the circumference was the zero crossing as shown in Figure 6. The luminance of the resulting pattern was set so that the zero crossings corresponded to the neutral gray of the monocular fields. Each probe stimulus is designated in terms of the spatial frequency of the component sine wave, which is the peak frequency of the probe. Four spatial frequencies were tested: 8.48, 4.24, 2.12, and 1.06 cycles per degree, which corresponded to probe diameters of 0.47, 0.94, 1.89, and 3.77 degrees of visual angle, respectively. The Michelson contrast of each probe was defined in terms of the maximum and minimum luminances of the probe, which were the two extreme luminance points one-quarter cycle distance from the center of the probe as shown in Figure 6.

Temporally, the contrast of the probes was modulated sinusoidally from zero contrast to peak contrast as shown in Figure 7, where the contrast of the probe is defined as the peak contrast. There were four temporal frequencies: 0, 3.75, 7.5, and 15 Hz. The 0 Hz probes were stationary. For the 3.75, 7.5, and 15 Hz probes, there were 16, 8, and 4 frames per cycle, respectively, where all the temporal frequency sequences included the peak and zero contrast frames (see Figure 7).

The contrast of the probe was under the subject's control; the contrast changes available were based on the limits of the 256 gray levels of the monitor. The contrasts of the stimuli were defined digitally by computer. However, because of nonlinearities between physical and digitally defined contrast, we measured the physical contrasts for each of the digitally defined contrasts for every spatial and temporal frequency variation of each probe stimulus. This was done by measuring the peak and trough at each contrast step for each probe stimulus pattern. We used a photometer with a slit aperture, 25x8000 microns, with a 5X microscopic lens, where the long dimension of the slit was perpendicular to the sinusoidal variation of the probe pattern. To reduce noise, the temporally varying patterns were low

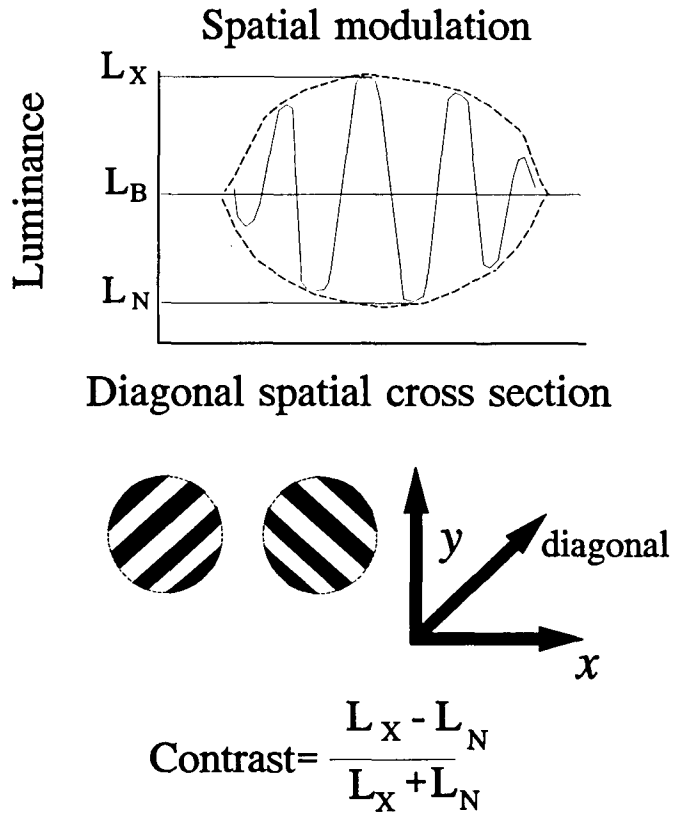

Figure 6. *Spatial modulation of probe stimuli. The probe stimuli were four cycles of a sine wave grating modulated by a circularly symmetric half cosine envelope (dashed lines) of 1/4 the spatial frequency of the sine wave. L_X represents the maximum luminance, L_N the minimum luminance, and L_B the mean (and the background) luminance of the resulting stimulus patch. The phase of the cosine envelope is 0° in the center, and the sine wave is randomly either 0° or 180°. These are modulated with respect to L_B. The top shows a diagonal cross section through one of the two probe stimulus orientations shown in the middle. Stimulus contrast is defined at the bottom. This represents the peak contrast for the temporally modulated patterns shown in Figure 7.*

passed with a cutoff at 30 Hz. The output signal was measured using a digital storage oscilloscope. We then curve fit second order regression equations to the digital to physical contrast function, which in all 16 cases was fit with at least 99.3 percent confidence, with most of the variation accounted for by the linear coefficients. The statistical analysis of the psychophysical data using either the digitally defined contrasts or the measured physical contrasts produced the same results. We report our results in terms of physical contrasts.

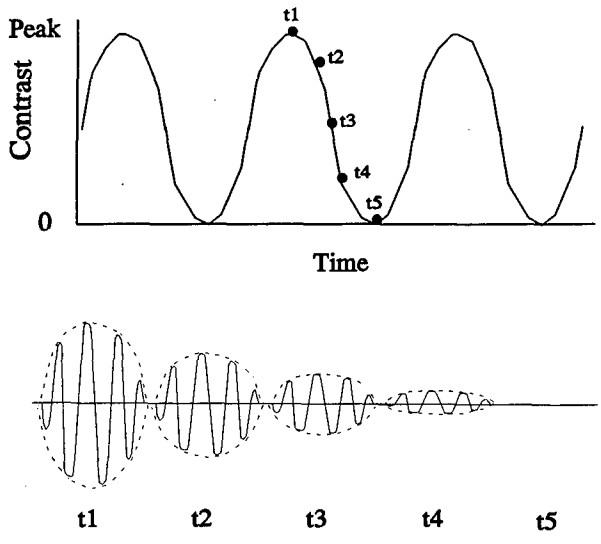

Figure 7. *Temporal modulation of probe stimuli. For the flickering probe stimuli, the contrast varied sinusoidally as shown on the top. Stimulus contrast is defined by the peak contrast. The bottom shows the luminance profile of a cross section of the probe at five points in time.*

Probe positions

The probes were centered vertically within the monocular fields and horizontally placed in one of four positions. Each of the four probe positions had symmetrical right-sided and left-sided versions with respect to the center of the display. Figure 8 shows the elliptical monocular fields of the three display modes and the left-sided versions of the four probe positions superimposed. Here the center ellipse represents the position of the monocular elliptical fields in the full overlap display mode and the ellipses to the right and left represent the positions in the partial overlap display modes as described in the caption. The four probe positions were the same in the three display modes, where the difference in the image was the positioning of the elliptical monocular fields. If the probe was positioned in the binocular region, it was present to both eyes; whereas, if it was positioned in a monocular region, it was present to only one eye.

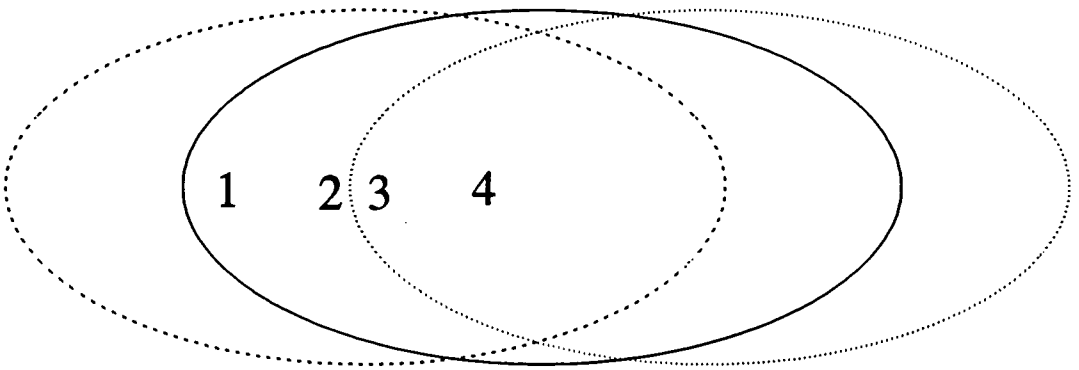

Figure 8. *The four probe positions. The relative positions of the elliptical monocular fields and the four probe positions are shown superimposed. Both eyes saw the ellipse with the solid line in the full overlap display mode. In the divergent display mode, the right eye saw the dotted ellipse on the right, and the left eye saw the dashed ellipse on the left. Conversely, in the convergent mode, the right eye saw the dashed ellipse on the left, and the left eye saw the dotted ellipse on the right.*

The four probe positions in the FOV were defined in terms of the distance from the binocular overlap border in the partial overlap display modes to the nearest edge of the probe. The distance between the edge of the probe and the binocular overlap border was the same for the different sized circular patches of the different spatial frequency probes.

The probes in positions 1 and 2 were monocular in the two partial overlap display modes and binocular in the full overlap mode. The probes in positions 3 and 4 were binocular in each of the three display modes. The probes in positions 2 and 3 were adjacent to the binocular overlap border in the two partial overlap display modes, the distance being 0.08 degrees of visual angle between the edge of the probe and the border. The probes in positions 1 and 4 were nonadjacent to the binocular overlap border in the two partial overlap display modes, the distance being 2.03 degrees of visual angle between the edge of the probe and the binocular overlap border. In the full overlap display mode, the probe positions were the same with respect to the center of the FOV; however, there was no binocular overlap border. Figure 9 shows all the probe position by display mode combinations.

Design

There were 192 different experimental conditions, which consisted of four probe spatial frequencies (8.48, 4.24, 2.12, and 1.06 cpd) x four probe temporal frequencies

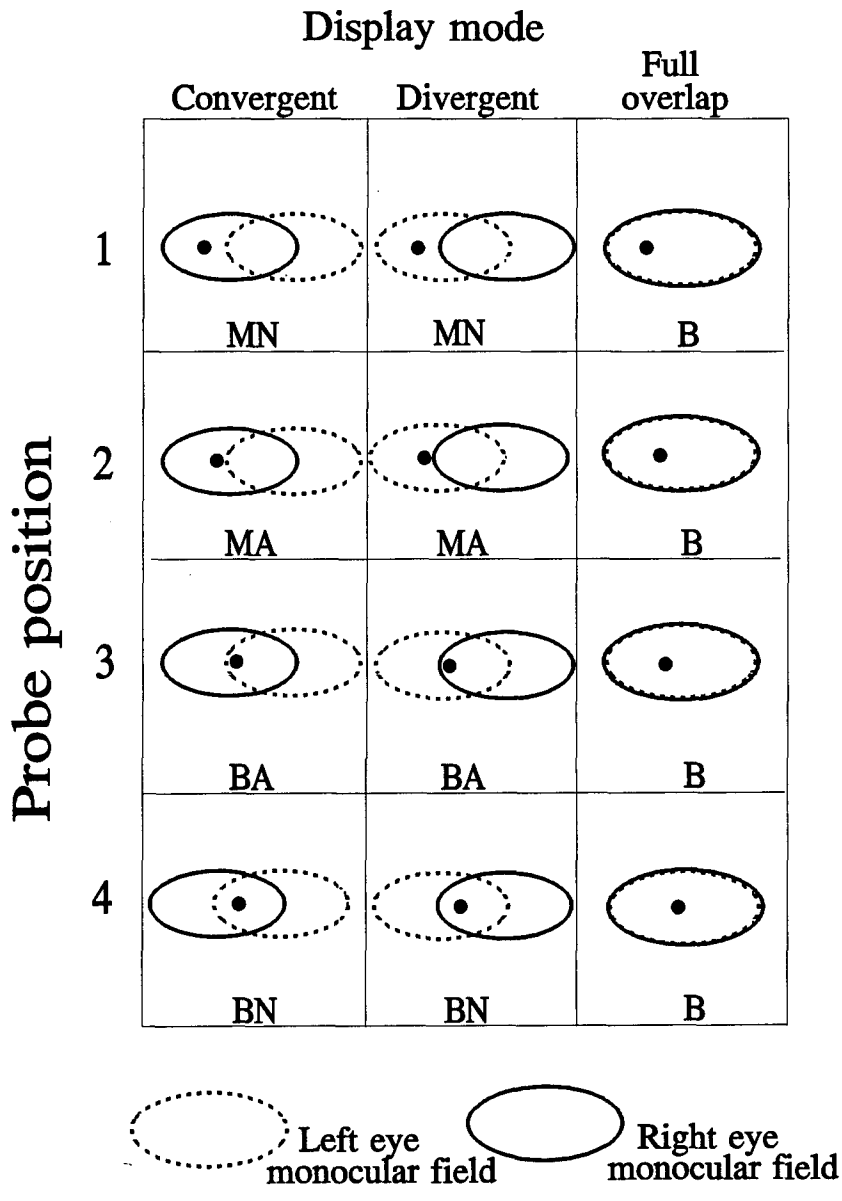

Figure 9. *Experimental displays. The left-sided versions of the four probe positions in the three display modes are shown. Positions 1 and 2 are monocular (M) in the convergent and the divergent display modes. The probes in the remaining position by display mode combinations are binocular (B). The probes in positions 2 and 3 in the convergent and divergent display modes are adjacent (A) to the binocular overlap border (0.08 degrees of visual angle). The probes in position 1 and 4 are nonadjacent (N) to the binocular overlap border (2.03 degrees of visual angle). There is no binocular overlap border in the full overlap display mode.*

(0, 3.75, 7.5, and 15 Hz) x four probe positions (positions 1, 2, 3, 4) x three display modes (convergent, divergent, and full overlap). These 192 experimental conditions were divided into 16 types of experimental session, where each session presented 1 of the 4 spatial frequencies at one of the four positions. These were seen under 12 experimental conditions, which consisted of the 4 temporal frequencies x the 3 display modes. The order of session type was randomized over subjects. Each subject took part in from one to 16 sessions over the course of a week based on availability from flight training school. The number of subjects completing each of the 16 sessions types varied from a minimum of 14 to a maximum of 27 (see Appendix C).

In each session, 24 trials were presented in random order within 3 blocks for a total of 72 trials. The 24 trials consisted of the right-sided and the left-sided versions of one probe position for 12 experimental conditions (4 temporal frequencies x 3 display modes).

Procedure

Each subject was required to read and sign the appropriate consent form explaining the task and the use of the button box. During experimental sessions, subject were seated in the dark in the subject booth, where they viewed the computer generated stimuli through a set of binoculars. The binoculars and movable mirrors, L4 and R4, were positioned individually to correspond to each subject's IPD. Each subject's head and eye were positioned properly by displaying an alignment pattern, a square grid which covered the entire extent of the screen, to ensure that the subject could see the entire screen through the binoculars. The subject first was given practice in obtaining binocular fusion and in the use of the button box, and before the first session was given a brief practice session with four or five stimuli, to make sure the instructions were understood. Before and after each session, the subject's phoria was measured for each of the three display modes.

A modified method of adjustment was used to set the contrast threshold for each stimulus trial. Each subject used five buttons of the button box to control the experiment. One button raised contrast of the stimulus probe in the minimal contrast steps available while a second button lowered contrast three steps. After threshold was set, a third button initiated a new trial. The fusion stimulus pattern could be called up and released by two additional buttons.

Only one probe position, right- and left-sided versions, was presented in a session. Subjects knew where to foveate to see the target. For each trial when the display came on, a stimulus locator appeared in the location of the stimulus probe for 250 milliseconds, then disappeared. This was to inform the subject as to whether the stimulus was a right- or a left-sided version of the position. The stimulus locator was a black square with a hole the size of the expected stimulus. The side of the square was the same size as the diameter of the hole. Two hundred and fifty milliseconds after the locator disappeared, the stimulus probe came on. The probe started at the zero contrast point of the temporal cycle for the temporally

modulated stimuli. For each trial, the contrast of the stimulus probe initially was set to zero. Each subject was instructed to raise the contrast via the button box to the lowest contrast at which the orientation of the stimulus probe could be identified. If the subject overshot the threshold by changing the contrast too fast, the contrast could be set back three steps. After each change in contrast, the probe reappeared at the new contrast randomly in one of its four versions---in one of two orientations and at one of two phases as described above. At the initiation of a new trial, the entire screen went blank for 250 milliseconds and a new trial started.

Subjects were told to respond only when the image was properly fused, which was indicated by the perception of only four fixation locks. They were told that if at any time during the presentation of a stimulus they lost fusion or became fatigued, they were to bring up the fusion stimulus pattern. After the fusion release button was pressed, the trial was restarted at the last contrast level with a new random probe phase and orientation.

Sessions lasted between 20 minutes and 1 hour, with the higher spatial frequency sessions generally lasting longer due to the greater number of steps needed to reach threshold. There was always at least an hour break between sessions to avoid fatigue, and at the most three sessions were run in a day.

Data analysis

Contrasts of the probe targets were controlled by each subject, where the step size for each increment of contrast was the smallest level of contrast change available. Each digital contrast threshold response was recorded by the computer and transformed into physical contrast based on our photometric measurements. Right- versus left-sided position bias was checked by performing a series of t-tests on the thresholds for each spatial frequency and temporal frequency and position combination for each of the three display modes. None of these were significant indicating no asymmetry in thresholds due to position side for any of the stimulus combinations.

Analysis of variance (Winer, 1971) was performed for each spatial frequency and temporal frequency and position combination, where the data were the mean, over subjects, of the contrast thresholds for each of the three display modes. Each subject's response was the mean of six responses (three blocks x right- and left-sided positions). If the analysis of variance was significant ($p<.05$), three t-tests were performed to test the following hypotheses. One, we tested the hypothesis that the thresholds were higher in the divergent display mode compared to the convergent display mode. This was because of the increased luning in the divergent case. Two and three, we tested the hypotheses that thresholds were higher in each of the partial binocular overlap display modes compared to the full overlap display mode. This was because of the predicted interference of dichoptic competition in the partial overlap modes, as well as the difference between monocular and binocular thresholds.

In parallel to the above analysis, we also performed the following analysis. Instead of using the contrasts for each of the three display conditions as input data, we analyzed contrast ratios. The data for each of the three conditions were the ratio of the contrast obtained in that condition over the contrast obtained in the full overlap condition. Thus for the convergent condition, the ratio was the convergent contrast divided by the full overlap contrast. Similarly for the divergent condition, the ratio was the divergent contrast divided by the full overlap contrast. In the full overlap condition, the ratio was one. For positions 1 and 2, the convergent and divergent data each represent the monocular over the binocular contrast ratio. These ratios were obtained for each subject before averaging the data across subjects for the statistical analysis. This analysis was done as a check on the data to ensure that there were no spurious results due to the group averages in the first analysis. Except for slight differences in significance levels, the results obtained from this analysis were the same in all cases as the results obtained with the original analysis reported below. The results of this analysis are therefore not reported separately.

Results and discussion

Contrast thresholds

The mean thresholds (and standard errors) for each position, temporal frequency, and display mode, are given in Tables C1-C4 in Appendix C and plotted in Figures D1-D16 in Appendix D. The associated statistical tests are given in Tables C5-C8 in Appendix C. In the tables, the experimental conditions are grouped by the session type in which they were presented. Figures D1-D16 plot the threshold results against position for the 3 display modes with each figure representing one of the 16 spatial frequency-temporal frequency combinations. Also, the contrast change step size available for the particular spatial frequency-temporal frequency combination is given in each figure. The probability values of the statistical tests, taken from Tables C5-C8, are given again at the bottom of these figures. Except for the absolute magnitudes of the thresholds, the results for the different temporal frequencies of each spatial frequency follow the same general pattern and are not discussed separately in detail.

The results for the lowest spatial frequency (1.06 cpd) probe targets are given in Tables C1 and C5 and Figures D1-D4. For positions 3 and 4, where all the probes were binocular, there were no significant differences between thresholds for the three display modes. When the targets were located in the monocular regions of the partial binocular overlap display modes, in positions 1 and 2, the thresholds were higher than they were for the corresponding binocular targets in the full overlap display mode. This was expected as monocular targets are known to have higher thresholds than binocular targets (Campbell and Green, 1965). For each temporal frequency the monocular thresholds in the partial overlap modes were higher than the thresholds in the corresponding binocular positions of the full overlap mode. There were no systematic differences between the two partial overlap modes for this spatial frequency.

The results for the next to lowest spatial frequency (2.12 cpd) probe targets are given in Tables C2 and C6 and Figures D5-D8. For position 4 again there were no significant differences between thresholds for the three display modes. In position 3, there were tiny elevations in threshold in the partial overlap modes compared to the full overlap mode for all but the 3.75 Hz temporal frequency. Elevation in threshold of the divergent mode over the convergent mode tended to be small and not statistically signifcant. All these differences were exceedingly small and inconsequential in light of the contrast changes step size as indicated in Figures D5-D8. In positions 1 and 2, there were no statistically significant differences between the divergent and the convergent display modes. However, again as with the lowest spatial frequency, when the targets were located in the monocular regions of the partial binocular overlap display modes, in positions 1 and 2, the thresholds were higher than they were in the corresponding binocular positions of the full overlap mode.

The results for the next to highest spatial frequency (4.24 cpd) probe targets are given in Tables C3 and C7 and Figures D9-D12. For position 4, there were no significant differences between thresholds for the three display modes. In position 3, even though all the probes were binocular, there were slight, but systematic, elevations in threshold in the partial overlap modes compared to the full overlap mode, and the thresholds in the divergent mode tended to be slightly higher than in the convergent mode. The differences reflecting this trend were very small in terms of contrast and of varying statistical significance across temporal frequency. There may have been a small influence of the presence of the adjacent binocular overlap border in the partial overlap modes, where this influence was slightly more detrimental in the divergent than in the convergent display mode. Again, when the targets were located in the monocular regions of the partial binocular overlap display modes, in positions 1 and 2, the thresholds of the probes were significantly higher than in the corresponding binocular positions of the full overlap mode. Again, for positions 1 and 2, the thresholds were higher in the divergent than in the convergent display mode, although they were significantly higher only for position 2 for two of the four temporal frequencies tested.

The results for the highest spatial frequency (8.48 cpd) probe targets are given in Tables C4 and C8 and Figures D13-16. For positions 3 and 4, where all the probes were binocular, there were no significant differences between thresholds for the three display modes. This indicates that presenting the FOV in the partial binocular overlap display mode does not appear to be deleterious to these small targets located in the binocular overlap region. However, when these targets were located in the monocular regions of the partial binocular overlap display modes---in positions 1 and 2--- all the thresholds, for each temporal frequency, were significantly higher in the two partial overlap modes than in the corresponding binocular positions of the full overlap mode. Again, this was as expected (Campbell and Green, 1965). In both positions 1 and 2, the thresholds were significantly higher in the divergent than in the convergent display mode. This was as expected from previous work showing that luning is more severe in the divergent mode than in the convergent mode (Moffitt, 1989; Klymenko et al., 1994b). It is noteworthy that the effects of luning extended out to position 1. The results for positions 1 and 2, showing an increase in threshold of the probe for the divergent over the convergent mode, was most clear cut for

this, the highest spatial frequency. Currently, we do not know for certain if this is a specific spatial frequency tuning effect or if at the lower frequencies, we were unable to measure the differences due to the lower limits of contrast changes---step sizes---available on our monitor. It is also noteworthy that in all cases, the thresholds in the partial overlap display modes increased in position 2 with respect to position 1, which is more distant from the overlap border. This may have been due to the decrease of luning away from the border (see Moffitt, 1989; Klymenko et al., 1994b).

Summary of results

In position 4, where the probe in each of the display modes was binocular and not adjacent to the binocular overlap border as in the partial overlap display modes, there were no differences in the thresholds for any of the probe targets at any of the spatio-temporal frequency combinations. In position 3, where the probes in each of the display modes was binocular, but were adjacent to the binocular overlap border as in the partial overlap display modes, there were some small differences in the thresholds at the two intermediate spatial frequencies. For all spatial and temporal frequencies, the probes in positions 1 and 2, as expected (Campbell and Green, 1965), had significantly higher thresholds in both of the partial overlap display modes, where the probes were monocular, compared to the full overlap display mode, where the probes were binocular.

We might expect differences in contrast threshold to probe stimuli presented monocularly to one eye versus probe stimuli presented to both eyes; however, we also found systematic increases in threshold for the divergent compared to the convergent display mode for the highest spatial frequency. It should be noted here that when these display patterns are viewed through the binoculars, subjects do not know if they are seeing a convergent or a divergent display. Subjectively, it appears to be a central binocular region with flanking monocular regions. It may be that the luning phenomenon, emanating from the border, and which is greater in the divergent display mode compared to the convergent display mode, may be related to this decrement in sensitivity. With our stimulus conditions, this effect is most pronounced for small high spatial frequency targets.

Discussion

The results on the increase in threshold for the probes in the partial overlap modes compared to the full overlap modes for positions 1 and 2, that is the increase in thresholds for the monocular probes compared to the binocular probes, was not surprising (Campbell and Green, 1965). As for the larger increases in threshold for position 2 relative to position 1, edges are strong dichoptic competitors that pull in neighboring regions into the binocular percept (Kaufman, 1963, 1964); thus distance to the binocular overlap border would be expected to be a factor. The relative contribution of the noninformational eye is greater the closer the probe is to the edge. In the cases where there was an increase in threshold for the

probes in the partial overlap modes compared to the full overlap modes for position 3, where all the probe conditions were binocular, the relevant factor may again have been the nearness of the binocular overlap border. This is not totally unexpected as the proximity of edges in general is known to decrease sensitivity to nearby stimuli (e.g., Fry and Bartley, 1935). This factor would not produce any differential effect on thresholds in position 4 deep in the binocular overlap region, where all the probes were binocular and nonadjacent to any borders.

The parallelism between the threshold results and the luning phenomenon in the partial overlap display modes implicates the processes of dichoptic competition and binocular rivalry and suppression. We discuss this elsewhere (Klymenko et al., 1994a, 1994b), where the phenomenon of luning and the related effect of fragmentation are considered in more detail. In brief, the divergent and the convergent display modes appear to differentially bias the visual system's interpretation of its input. The visual system appears in both cases to settle on likely real world configurations corresponding to the input, and appropriate processing mechanisms may therefore be activated (see Melzer and Moffitt, 1991). Possible configurations for the divergent and the convergent display modes are shown in Figures 10 and 11 respectively. For example, the convergent mode induces less luning maybe because it is more ecologically valid, that is, closer to a natural viewing situation. The convergent mode simulates viewing the visual world through an aperture. Another possible reason for these results may be the visual system's normal role in suppressing diplopia of off-fixation points (see Figure 12). Here, greater importance is assigned to off-fixation points in near space leading to greater suppression of the far background image in dichoptic competition with these points compared to points in far space. This may explain the differential thresholds between the divergent and the convergent display mode (Klymenko et al., 1994a). More research is needed to tie together the underlying connections between luning, fragmentation, the visual thresholds reported here, and the processing biases of the visual system induced by helmet mounted display modes.

Acknowledgement: We thank Dr. Roger W. Wiley for his scientific review and Udo Volker Nowak for his editorial review.

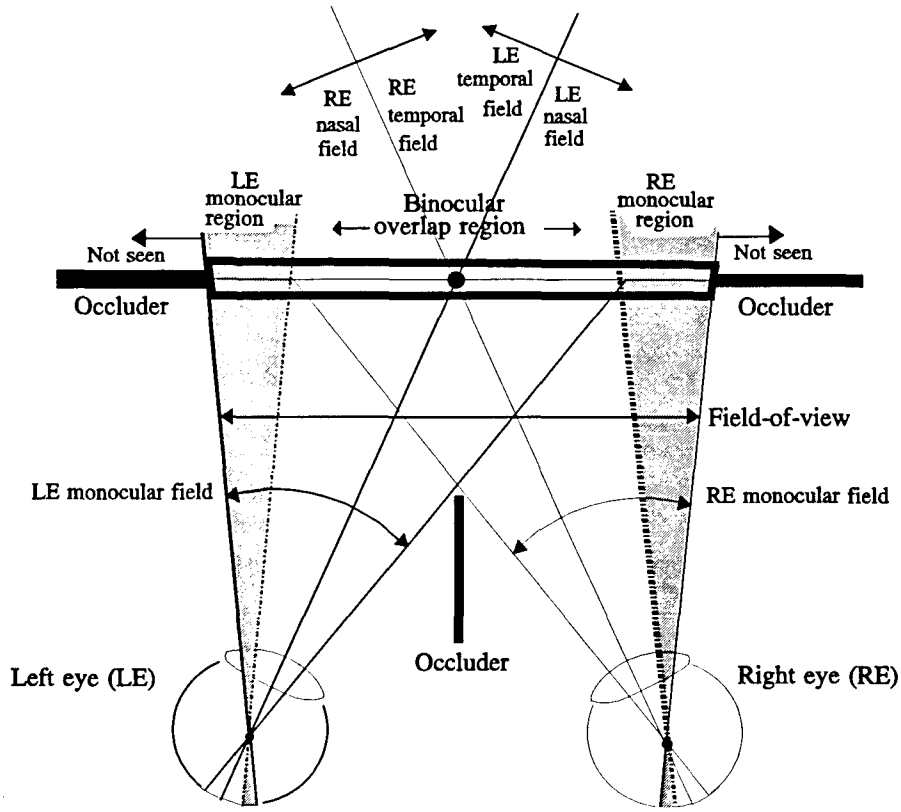

Figure 10. *Visual geometric interpretation of the divergent display mode. Shown is the top view of one of the possible geometric configurations the visual system may be biased to interpret when presented with a divergent display in a helmet mounted display. The dark backgrounds are seen as occluders in space and the field-of-view is seen ambiguously as either a projected image or as the visual world through an aperture. Visually each monocular region of the field-of-view is the binocular result of dichoptic competition between a part of the monocular field projected onto one retina with the part of the background projected onto the corresponding retinal area of the contralateral eye.*

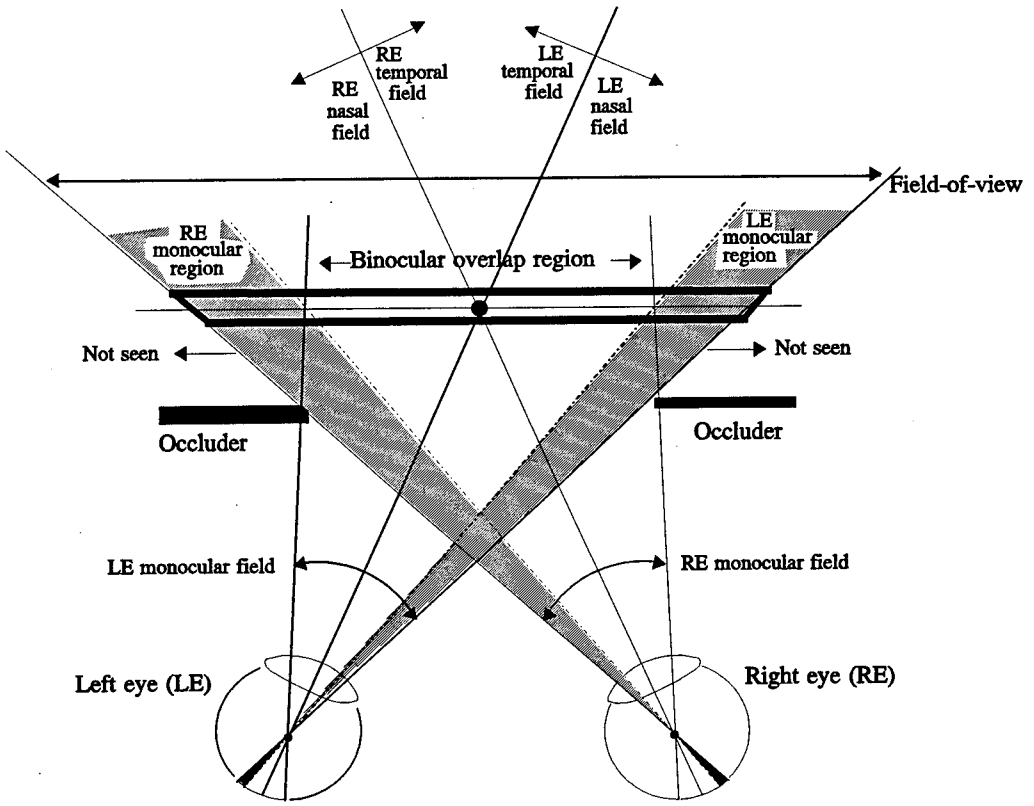

Figure 11. *Visual geometric interpretation of the convergent display mode. Shown is a top view of one of the possible geometric configurations the visual system may be biased to interpret when presented with a convergent display in a helmet mounted display. The field-of-view is seen as the visual world occluded by the borders of an aperture. Visually each monocular region of the field-of-view is the binocular result of dichoptic competition between a part of the monocular field projected onto one retina with the part of the background projected onto the corresponding area of the contralateral eye.*

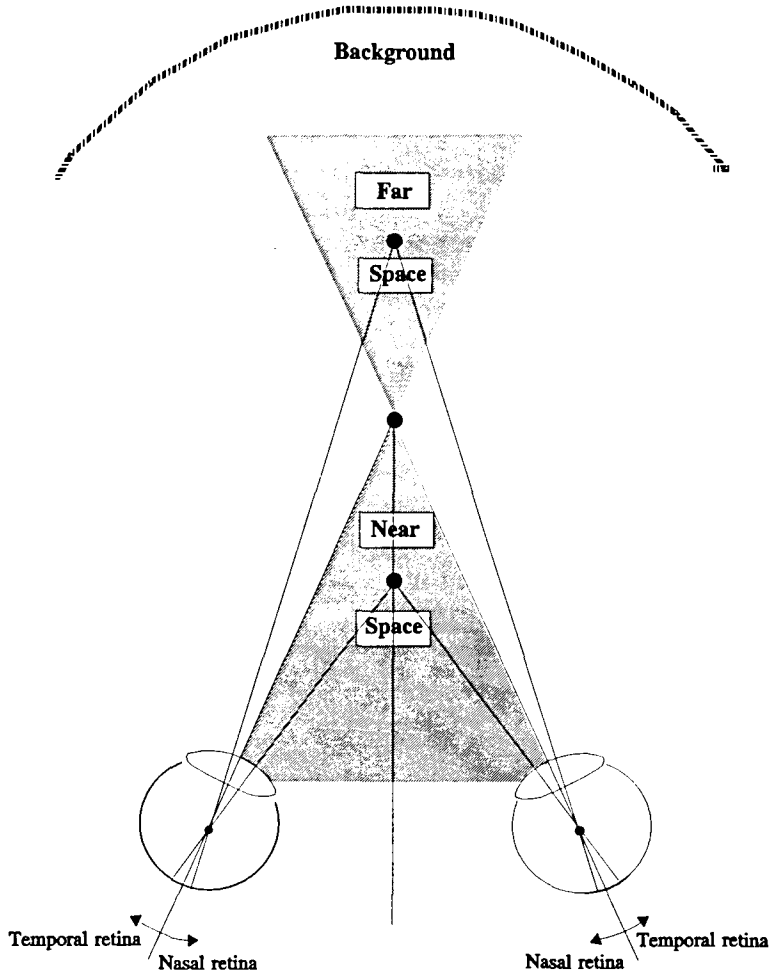

Figure 12. *Retinal projection of the fixation point and off-fixation points in near space and far space. Symmetrical image points on the nasal retinas representing object points in far space are in dichoptic competition with corresponding points on the contralateral temporal retinas representing the far background. Conversely, symmetrical image points on the temporal retinas representing object points in near space are in dichoptic competition with corresponding points on the contralateral nasal retinas representing the far background.*

References

Alam, M. S., Zheng, S. H., Iftekharuddin, K. M., and Karim, M. A. 1992. Study of field-of-view overlap for night vision applications. Proceeding of the 1992 IEEE National Aerospace and Electronics Conference, NEACON Vol 3, 1249-1255. Dayton, OH.

Arditi, A. 1986. Binocular vision. In (K. R. Boff, L. Kaufman, and J. P. Thomas) Handbook of perception and human performance, Vol. 1. New York: John Wiley & Sons.

Boff, K. R., and Lincoln, J. E. 1988. Engineering data compendium: human perception and performance. Wright-Patterson Air Force Base, OH: Armstrong Aerospace Medical Research Laboratory.

CAE Electronics. 1984. Wide-field-of-view, helmet-mounted infinity display system development, Brooks Air Force Base, TX: Air Force Systems Command. AFHRL-TR-84-27.

Campbell, F. W., and Green, D. G. 1965. Monocular versus binocular visual acuity. Nature, 208, 315-323.

Campbell, F. W., and Robson, J. G. 1968. Application of Fourier analysis to the visibility of gratings. Journal of physiology, 197, 551-566.

Edgar, G. K., Carr, K. T., Williams, M., and Clark, A. L. 1991. The effect upon visual performance of varying binocular overlap. AGARD symposium on helmet-mounted displays and night vision goggles, Neuilly-sur-Seine, France. (AGARD Conference Proceedings 517), 8-1 to 8-15.

Farrell, R. J., and Booth, J. M. 1984. Design handbook for imagery interpretation equipment. Seattle, WA: Boeing Aerospace Co.

Fry, G. A., and Bartley, S. H. 1935. The effect of one border in the visual field upon the threshold of another. American journal of physiology, 112, 414-421.

Gibson, J. J. 1979. The ecological approach to visual perception. Boston, MA: Houghton-Mifflin.

Kaufman, L. 1963. On the spread of suppression and binocular rivalry. Vision research, 3, 401-415.

Kaufman, L. 1964. Suppression and fusion in viewing complex stereograms. American journal of psychology, 77, 193-205.

Kenyon, R. V., and Kneller, E. W. 1993. The effects of field of view size on the control of roll motion. IEEE transactions on systems, man, and cybernetics, 25(1), 183-193.

Klymenko, V., Verona, R. W., Beasley, H. H., Martin, J. S., and McLean W. E. 1994a. Factors affecting the visual fragmentation of the field-of-view in partial binocular overlap displays. Fort Rucker, AL: U.S. Army Aeromedical research Laboratory. USAARL report no. 94-29.

Klymenko, V., Verona, R. W., Martin, J. S., Beasley, H. H., and McLean W. E. 1994b. Factors affecting the perception of luning in monocular regions of partial binocular overlap displays. Fort Rucker, AL: U.S. Army Aeromedical research Laboratory. USAARL report no. 94-47.

Kruk, R., and Longridge, T. M. 1984. Binocular Overlap in a fiber optic helmet mounted display. The image 3 conference proceedings, 363, 363-377. Brooks Air Force Base, TX: Air Force Human Resources Laboratory, Air Force Systems Command. AFHRL-TR-84-36.

Landau, F. 1990. The effect on visual recognition performance of misregistration and overlap for a biocular helmet mounted display. SPIE proceedings, Vol. 1290, helmet-mounted displays II, 173-184. San Jose, CA: SPIE-The International Society for Optical Engineering.

Melzer, J. E., and Moffitt, K. 1989. Partial binocular overlap in helmet-mounted displays. SPIE Proceedings, Vol. 1117, display system optics II, 56-62. San Jose, CA: SPIE-The International Society for Optical Engineering.

Melzer, J. E., and Moffitt, K. 1991. An ecological approach to partial binocular-overlap. SPIE proceedings, Vol. 1456, large screen projection, ionic, and helmet-mounted displays, 175-191. San Jose, CA: SPIE-The International Society for Optical Engineering.

Moffitt, K. 1989. Luning and target detection. San Jose, CA: Kaiser Electronics.

Moffitt, K. 1991. Partial binocular overlap: concepts, research, & systems. San Jose, CA: Kaiser Electronics.

Moffitt, K., and Melzer, J. 1991. Partial binocular overlap. San Jose, CA: Kaiser Electronics.

Nakayama, K. 1985. Biological image motion processing: A review. Vision research, 25, 625-660.

Osgood, R. K., and Wells, M. J. 1991. The effect of field-of-view size on performance of a simulated air-to-ground night attack. AGARD symposium on helmet-mounted displays and night vision goggles (AGARD Conference Proceedings 517), 10-1 to 10-7., Aerospace medical panel symposium, Pensacola, FL.

Plant, G. T. 1991. Temporal properties of normal and abnormal vision. In (D. Regan), Vision and visual dysfunction, Vol. 10., 43-63.

Wells, M. J., Venturino, M., and Osgood, R. K. 1989. The effect of field-of-view on performance at a simple simulated air-to-air mission. SPIE proceedings, Vol. 1116, helmet-mounted displays, 126-137. San Jose, CA: SPIE-The International Society for Optical Engineering.

Winer, B. J. 1971. Statistical principles in experimental design. New York: McGraw-Hill.

Wolpert, L. 1990. Field-of-view information for self-motion perception. In (R. Warren and A. H. Wertheim) Perception and control of self-motion. Hillsdale, NJ: Lawrence Earlbaum Associates.

Appendix A.

Eye exam data sheet

Psychophysical Assessment of Visual Parameters in Electro-optical Display Systems

VISUAL EXAM

Subject #_____ Age:_____ Date:_____

Old RX: R.E._____ L.E._____
for distant vision (Yes) (No)
for near vision (Yes) (No)
Bifocal (Yes) (No)

AFVT - with glasses if required for distance #3, #2, #1

VA R.E. line_____20/____ Lateral Phoria #____ _____
FAR L.E. line_____20/_____ Vertical Phoria #____ _____
LP = XO >11; VP = Rt Hyper >5, .5 steps

Stereopsis thru line# _____
Lateral Phoria @ Near #_____ _____ LP = XO >13

AUTO REFRACTION (ARK 2000) P.D. _____

O.D. _____
O.S. _____

SUBJECTIVE REFRACTION: (Green>Red) X-CYL at far
O.D. _____ 20/ O.D._____ SPH
O.S. _____ 20/

Lateral Phoria @ Far _____ Vertical Phoria_____

Lateral Phoria @ Far with -1.00 D _____

Lateral Phoria @ 50 cm _____ X-CYL @ 50 cm O.D._____SPH
Lateral Phoria @ 50 cm +1.00 D _____
Lateral Phoria @ 50 cm -1.00 D _____
Calculated ACA ratios far minus _____
near plus _____
near minus_____

Appendix B.

Manufacturers' List

Hewlett-Packard Company
3404 East Harmony Road
Fort Collins, CO 80525

Edmund Scientific Co.
Edscorp Building
Barrington, NJ 08807

Appendix C.

Results tables

Table C1.
Contrast thresholds for spatial frequency 1.06 cycles per degree: means and standard errors.

Position	Temporal frequency (Hz)	Display mode: Convergent mean (SE)	Display mode: Divergent mean (SE)	Display mode: Full overlap mean (SE)	Number of subjects
1	0	2.96 (0.16)	2.80 (0.16)	2.43 (0.17)	18
	3.75	5.99 (0.11)	6.00 (0.10)	5.54 (0.11)	
	7.5	6.36 (0.09)	6.35 (0.09	6.01 (0.12)	
	15	6.58 (0.15)	6.53 (0.13)	6.02 (0.11)	
2	0	2.88 (0.13)	2.91 (0.12)	2.40 (0.14)	20
	3.75	6.20 (0.11)	6.17 (0.12)	5.46 (0.10)	
	7.5	6.59 (0.14)	6.53 (0.11)	6.05 (0.11)	
	15	6.76 (0.17)	6.72 (0.14)	6.15 (0.13)	
3	0	2.00 (0.10)	2.09 (0.12)	1.99 (0.11)	17
	3.75	5.17 (0.11)	5.24 (0.11)	5.06 (0.10)	
	7.5	5.69 (0.09)	5.68 (0.10)	5.61 (0.09)	
	15	5.66 (0.04)	5.69 (0.08)	5.65 (0.04)	
4	0	2.15 (0.16)	2.14 (0.16)	2.11 (0.14)	14
	3.75	5.27 (0.16)	5.23 (0.15)	5.27 (0.13)	
	7.5	5.68 (0.14)	5.62 (0.14)	5.70 (0.15)	
	15	5.76 (0.15)	5.70 (0.11)	5.76 (0.11)	

Table C2.
Contrast thresholds for spatial frequency 2.12 cycles per degree: means and standard errors.

Position	Temporal frequency (Hz)	Display mode: Convergent mean (SE)	Display mode: Divergent mean (SE)	Display mode: Full overlap mean (SE)	Number of subjects
1	0	2.27 (0.17)	2.22 (0.16)	1.88 (0.15)	23
	3.75	6.24 (0.17)	6.16 (0.13)	5.71 (0.12)	
	7.5	6.31 (0.19)	6.28 (0.18)	5.93 (0.14)	
	15	6.63 (0.22)	6.65 (0.18)	6.12 (0.14)	
2	0	2.29 (0.12)	2.44 (0.11)	1.90 (0.09)	27
	3.75	6.35 (0.14)	6.55 (0.16)	5.88 (0.12)	
	7.5	6.59 (0.14)	6.69 (0.13)	6.00 (0.13)	
	15	6.89 (0.17)	6.95 (0.16)	6.21 (0.12)	
3	0	1.64 (0.10)	1.72 (0.11)	1.49 (0.10)	25
	3.75	5.53 (0.08)	5.62 (0.11)	5.51 (0.08)	
	7.5	5.74 (0.10)	5.80 (0.11)	5.62 (0.10)	
	15	5.97 (0.12)	6.02 (0.11)	5.86 (0.10)	
4	0	1.63 (0.14)	1.69 (0.15)	1.62 (0.14)	21
	3.75	5.60 (0.11)	5.54 (0.13)	5.56 (0.11)	
	7.5	5.72 (0.14)	5.73 (0.12)	5.46 (0.10)	
	15	5.87 (0.12)	5.93 (0.12)	5.92 (0.13)	

Table C3.
Contrast thresholds for spatial frequency 4.24 cycles per degree:
means and standard errors.

Position	Temporal frequency (Hz)	Display mode: Convergent mean (SE)	Divergent mean (SE)	Full overlap mean (SE)	Number of subjects
1	0	3.61 (0.28)	3.65 (0.27)	3.14 (0.23)	22
	3.75	7.76 (0.33)	7.96 (0.30)	7.11 (0.23)	
	7.5	8.08 (0.34)	8.26 (0.36)	7.38 (0.28)	
	15	10.30 (0.42)	10.48 (0.34)	9.57 (0.27)	
2	0	3.50 (0.24)	4.02 (0.28)	3.00 (0.20)	26
	3.75	7.80 (0.28)	8.09 (0.35)	7.06 (0.23)	
	7.5	8.38 (0.37)	8.51 (0.40)	7.31 (0.27)	
	15	10.19 (0.32)	10.94 (0.42)	9.44 (0.26)	
3	0	3.32 (0.20)	3.36 (0.20)	3.09 (0.20)	26
	3.75	7.40 (0.21)	7.54 (0.22)	7.25 (0.20)	
	7.5	7.69 (0.25)	7.88 (0.29)	7.53 (0.25)	
	15	9.94 (0.28)	9.95 (0.29)	9.66 (0.26)	
4	0	2.88 (0.15)	2.89 (0.18)	2.88 (0.19)	19
	3.75	6.79 (0.15)	6.89 (0.17)	6.82 (0.13)	
	7.5	7.09 (0.16)	7.14 (0.19)	6.91 (0.17)	
	15	9.13 (0.19)	9.10 (0.18)	9.04 (0.17)	

Table C4.
Contrast thresholds for spatial frequency 8.48 cycles per degree: means and standard errors.

Position	Temporal frequency (Hz)	Display mode: Convergent mean (SE)	Display mode: Divergent mean (SE)	Display mode: Full overlap mean (SE)	Number of subjects
1	0	7.42 (0.71)	8.16 (0.74)	6.48 (0.49)	18
	3.75	12.45 (1.01)	13.28 (0.93)	11.34 (0.78)	
	7.5	12.69 (1.07)	14.14 (1.00)	11.80 (0.77)	
	15	13.58 (1.20)	14.91 (1.14)	11.93 (0.84)	
2	0	8.36 (0.54)	9.72 (0.64)	6.87 (0.45)	23
	3.75	13.52 (0.68)	15.19 (0.82)	11.59 (0.57)	
	7.5	14.28 (0.78)	15.82 (0.90)	12.34 (0.62)	
	15	14.77 (0.86)	17.04 (1.02)	13.13 (0.75)	
3	0	6.97 (0.51)	6.93 (0.52)	6.63 (0.51)	25
	3.75	11.79 (0.63)	11.93 (0.60)	11.46 (0.52)	
	7.5	12.81 (0.77)	12.79 (0.67)	12.11 (0.60)	
	15	13.34 (0.81)	12.74 (0.72)	12.61 (0.67)	
4	0	7.48 (0.63)	7.26 (0.61)	7.40 (0.63)	17
	3.75	12.22 (0.82)	11.87 (0.77)	12.09 (0.75)	
	7.5	13.09 (0.92)	12.39 (0.70)	12.56 (0.78)	
	15	13.04 (0.90)	12.62 (0.84)	12.78 (0.85)	

Table C5.
Statistical tests for spatial frequency 1.06 cycles per degree.

Position	Temporal frequency (Hertz)	ANOVA	p	t-tests df	C<D	p	F<C	p	F<D	p
1	0	F(2,34) = 18.03	<.001	17	-1.63	false	6.06	<.001	4.24	<.001
	3.75	F(2,34) = 27.56	<.001		0.14	=.442	6.42	<.001	6.87	<.001
	7.5	F(2,34) = 14.02	<.001		-0.18	false	4.07	<.001	4.16	<.001
	15	F(2,34) = 21.40	<.001		-0.54	false	5.00	<.001	6.29	<.001
2	0	F(2,38) = 18.22	<.001	19	0.28	=.391	5.90	<.001	5.39	<.001
	3.75	F(2,38) = 83.23	<.001		-0.44	false	13.39	<.001	9.50	<.001
	7.5	F(2,38) = 30.95	<.001		-0.84	false	7.03	<.001	6.33	<.001
	15	F(2,38) = 24.02	<.001		-0.49	false	5.53	<.001	5.92	<.001
3	0	F(2,32) = 1.26	n.s.							
	3.75	F(2,32) = 3.12	n.s.							
	7.5	F(2,32) = 1.32	n.s.							
	15	F(2,32) = 0.30	n.s.							
4	0	F(2,26) = 0.48	n.s.							
	3.75	F(2,26) = 0.28	n.s.							
	7.5	F(2,26) = 1.21	n.s.							
	15	F(2,26) = 0.70	n.s.							

Note: C = convergent display mode, D = divergent display, mode and F = full overlap display mode, df = degrees of freedom.

Table C6.
Statistical tests for spatial frequency 2.12 cycles per degree.

Position	Temporal frequency (Hertz)	ANOVA	p	t-tests df	C<D	p	F<C	p	F<D	p
1	0	F(2,44) = 14.49	<.001	22	-0.58	false	4.30	<.001	4.80	<.001
	3.75	F(2,44) = 33.72	<.001		-1.25	false	6.69	<.001	7.45	<.001
	7.5	F(2,44) = 13.08	<.001		0.42	=.338	4.34	<.001	3.88	<.001
	15	F(2,44) = 17.90	<.001		0.18	=.431	4.53	<.001	5.76	<.001
2	0	F(2,52) = 35.34	<.001	26	2.16	=.020	6.21	<.001	7.77	<.001
	3.75	F(2,52) = 15.53	<.001		1.43	=.082	5.82	<.001	4.97	<.001
	7.5	F(2,52) = 24.67	<.001		0.83	=.209	6.01	<.001	7.30	<.001
	15	F(2,52) = 31.03	<.001		0.57	=.285	6.14	<.001	7.52	<.001
3	0	F(2,48) = 12.44	<.001	24	1.87	=.036	3.89	<.001	4.16	<.001
	3.75	F(2,48) = 2.66	n.s.							
	7.5	F(2,48) = 7.60	<.005		1.05	=.151	2.79	=.005	3.91	<.001
	15	F(2,48) = 6.66	<.005		1.48	=.078	2.44	=.011	3.08	=.003
4	0	F(2,40) = 1.10	n.s.							
	3.75	F(2,40) = 1.00	n.s.							
	7.5	F(2,40) = 1.47	n.s.							
	15	F(2,40) = 1.16	n.s.							

Note: C = convergent display mode, D = divergent display mode, and F = full overlap display mode, df = degrees of freedom.

Table C7.
Statistical tests for spatial frequency 4.24 cycles per degree.

Position	Temporal frequency (Hertz)	ANOVA	p	t-tests df	C<D	p	F<C	p	F<D	p
1	0	F(2,42) = 8.28	<.001	21	0.25	=.404	4.36	<.001	3.41	<.001
	3.75	F(2,42) = 13.54	<.001		1.01	=.162	3.93	<.001	5.97	<.001
	7.5	F(2,42) = 14.33	<.001		0.85	=.202	5.42	<.001	5.29	<.001
	15	F(2,42) = 13.10	<.001		0.87	=.197	3.34	=.002	6.84	<.001
2	0	F(2,50) = 15.86	<.001	25	2.43	=.011	5.00	<.001	4.94	<.001
	3.75	F(2,50) = 17.39	<.001		1.40	=.087	6.16	<.001	5.09	<.001
	7.5	F(2,50) = 21.35	<.001		0.55	=.295	7.13	<.001	5.37	<.001
	15	F(2,50) = 17.00	<.001		2.59	=.008	6.08	<.001	4.79	<.001
3	0	F(2,50) = 4.65	<.05	25	0.55	=.294	2.18	=.020	2.69	=.006
	3.75	F(2,50) = 5.95	<.01		1.85	=.038	1.67	=.053	3.35	<.001
	7.5	F(2,50) = 4.37	<.05		2.07	=.024	1.28	=.107	2.62	=.007
	15	F(2,50) = 4.45	<.05		0.14	=.441	3.13	=.002	2.50	=.010
4	0	F(2,36) = 0.01	n.s.							
	3.75	F(2,36) = 1.09	n.s.							
	7.5	F(2,36) = 5.46	n.s.							
	15	F(2,36) = 0.67	n.s.							

Note: C = convergent display mode, D = divergent display mode, and F = full overlap display mode, df = degrees of freedom.

Table C8.

Statistical tests for spatial frequency 8.48 cycles per degree.

Position	Temporal frequency (Hertz)	ANOVA	p	t-tests df	C<D	p	F<C	p	F<D	p
1	0	F(2,34) = 10.48	<.001	17	2.07	=.027	2.76	=.007	4.18	<.001
	3.75	F(2,34) = 11.28	<.001		1.81	=.043	3.03	=.004	4.85	<.001
	7.5	F(2,34) = 12.61	<.001		2.66	=.008	2.02	=.030	5.61	<.001
	15	F(2,34) = 16.83	<.001		2.50	=.011	2.89	=.005	6.91	<.001
2	0	F(2,44) = 21.98	<.001	22	3.04	=.003	5.32	<.001	5.42	<.001
	3.75	F(2,44) = 31.19	<.001		3.62	<.001	5.50	<.001	6.71	<.001
	7.5	F(2,44) = 35.96	<.001		3.36	<.001	7.81	<.001	7.17	<.001
	15	F(2,44) = 31.08	<.001		4.24	<.001	5.53	<.001	6.43	<.001
3	0	F(2,48) = 1.96	n.s.							
	3.75	F(2,48) = 2.09	n.s.							
	7.5	F(2,48) = 3.14	n.s.							
	15	F(2,48) = 2.97	n.s.							
4	0	F(2,32) = 0.42	n.s.							
	3.75	F(2,32) = 0.86	n.s.							
	7.5	F(2,32) = 1.70	n.s.							
	15	F(2,32) = 1.43	n.s.							

Note: C = convergent display mode, D = divergent display mode, and F = full overlap display mode, df = degrees of freedom.

Appendix D.

Results figures

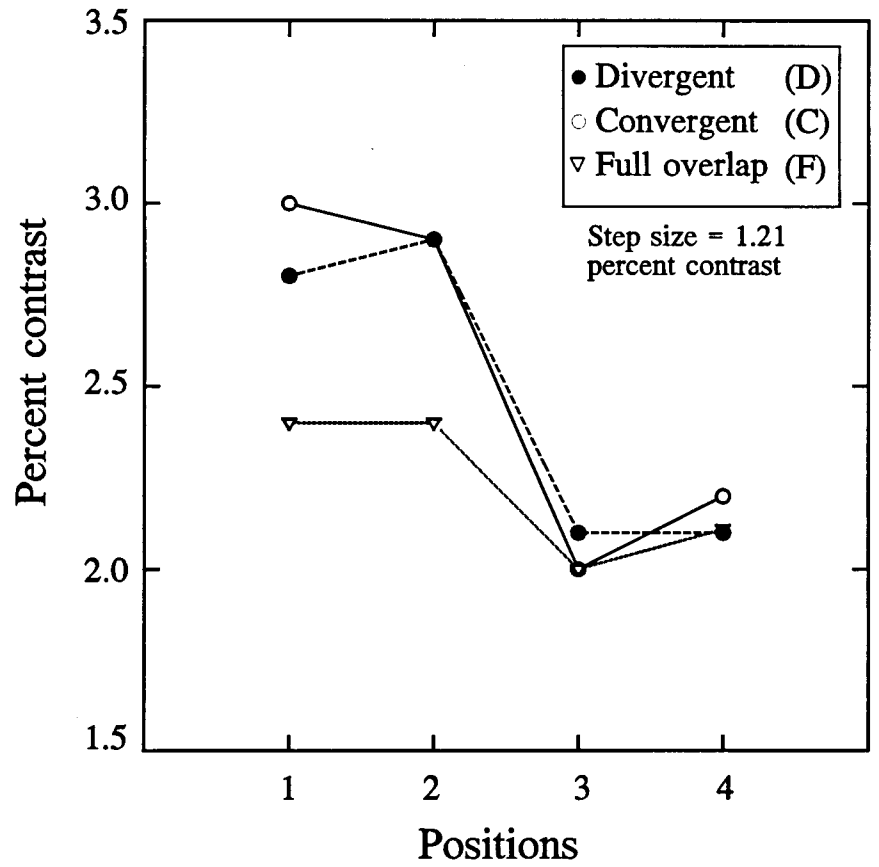

t - test	1	2	3	4
C<D	p=.061 f	p=.391 f	------	------
F<C	p<.001	p<.001	------	------
F<D	p<.001	p<.001	------	------
ANOVA	p<.001	p<.001	n.s.	n.s.

f = false

n.s.= not significant

Figure D1. *Thresholds for 1.06 cpd and 0 Hz. Means and standard errors of graphed data points are listed in Table C1. Bottom of figure shows results of statistical analyses from Table C5.*

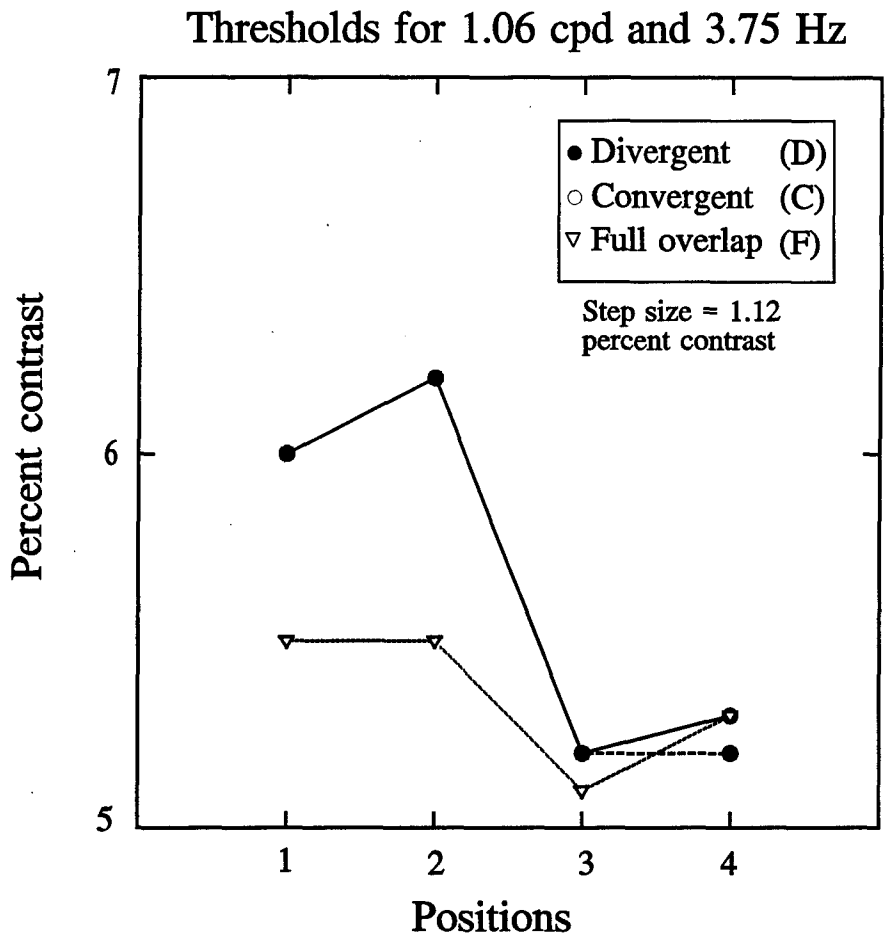

t - test	1	2	3	4
C<D	p=.442	p=.332 f	------	------
F<C	p<.001	p<.001	------	------
F<D	p<.001	p<.001	------	------
ANOVA	p<.001	p<.001	n.s.	n.s.

f = false

n.s.= not significant

Figure D2. *Thresholds for 1.06 cpd and 3.75 Hz. Means and standard errors of graphed data points are listed in Table C1. Bottom of figure shows results of statistical analyses from Table C5.*

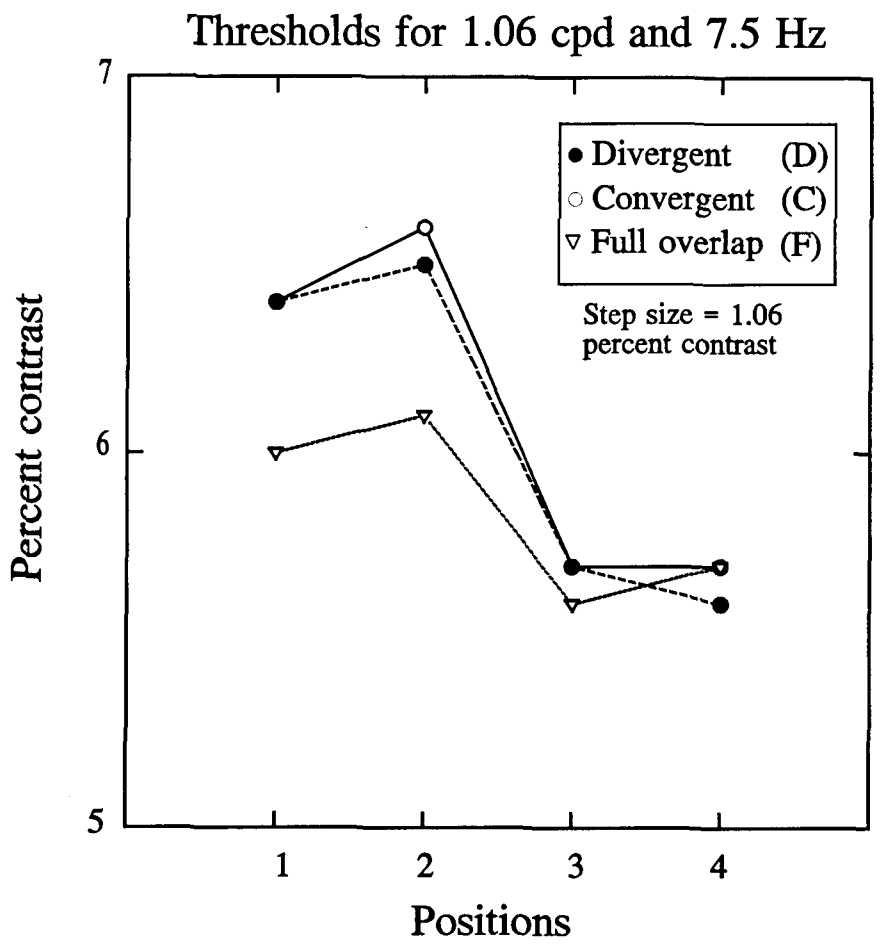

t - test	1	2	3	4
C<D	p=.436	p=.206 f	------	------
F<C	p<.001	p<.001	------	------
F<D	p<.001	p<.001	------	------
ANOVA	p<.001	p<.001	n.s.	n.s.

f = false

n.s.= not significant

Figure D3. *Thresholds for 1.06 cpd and 7.5 Hz. Means and standard errors of graphed data points are listed in Table C1. Bottom of figure shows results of statistical analyses from Table C5.*

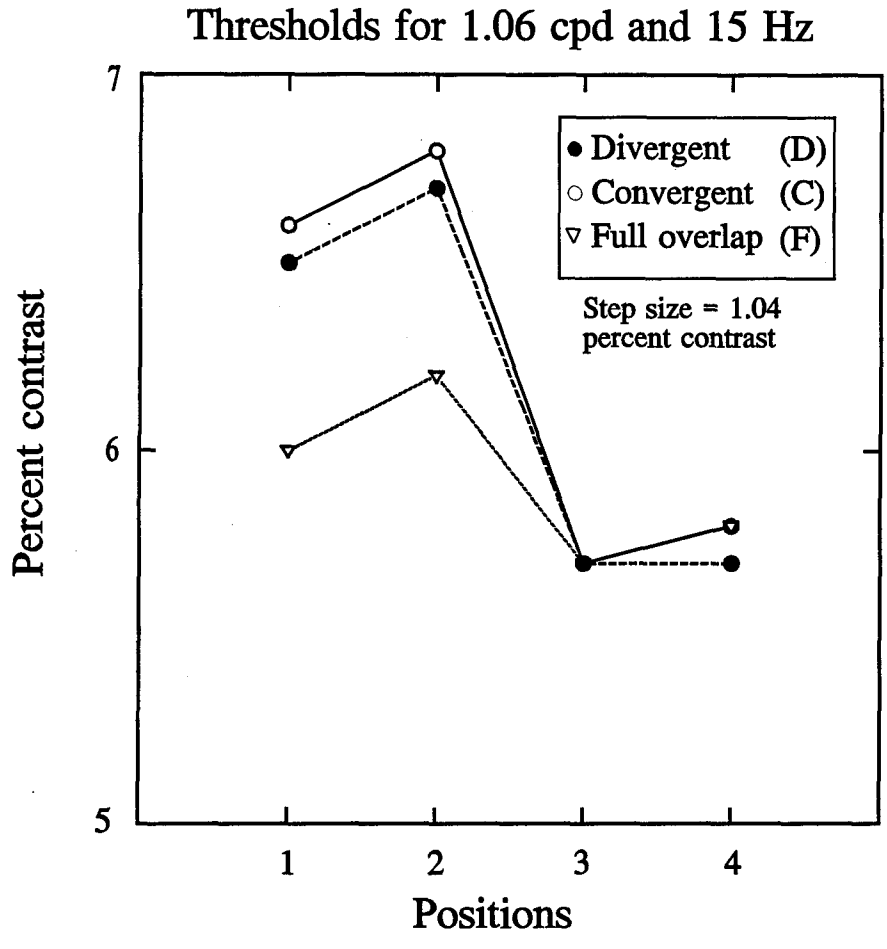

t - test	1	2	3	4
C<D	p=.291 f	p=.319 f	------	------
F<C	p<.001	p<.001	------	------
F<D	p<.001	p<.001	------	------
ANOVA	p<.001	p<.001	n.s.	n.s.

f = false

n.s.= not significant

Figure D4. *Thresholds for 1.06 cpd and 15 Hz. Means and standard errors of graphed data points are listed in Table C1. Bottom of figure shows results of statistical analyses from Table C5.*

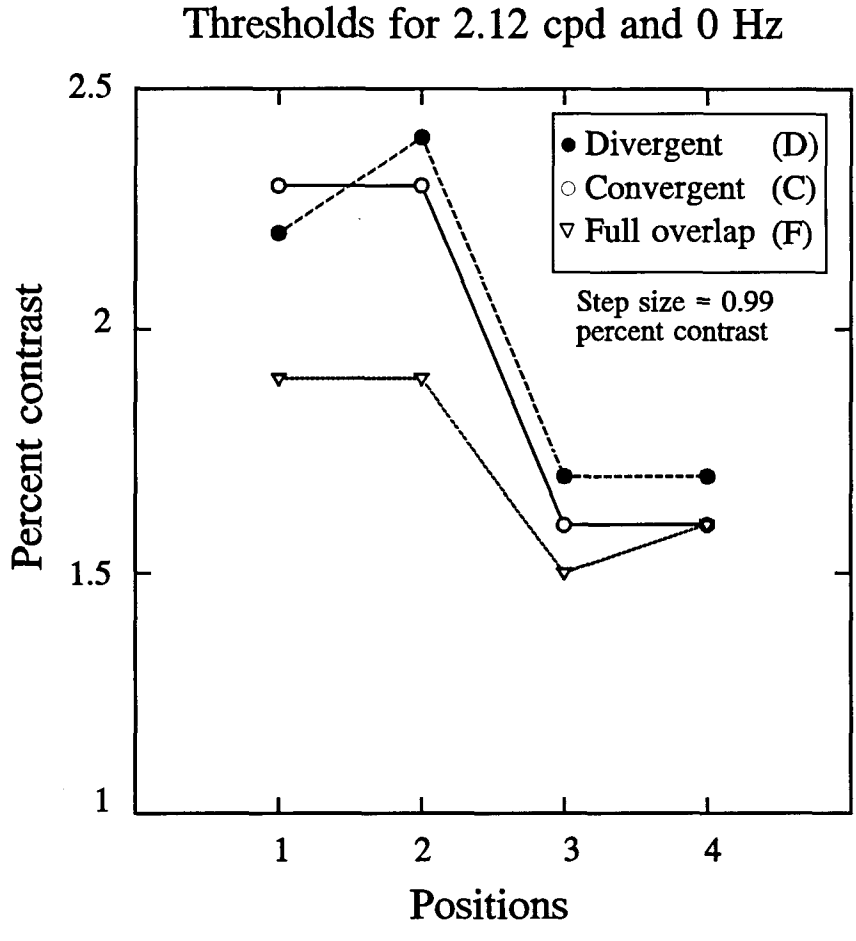

t - test	1	2	3	4
C<D	p=.278 f	p=.020	p=.036	------
F<C	p<.001	p<.001	p<.001	------
F<D	p<.001	p<.001	p<.001	------
ANOVA	p<.001	p<.001	p<.01	n.s.

f = false

n.s.= not significant

Figure D5. *Thresholds for 2.12 cpd and 0 Hz. Means and standard errors of graphed data points are listed in Table C2 Bottom of figure shows results of statistical analyses from Table C6.*

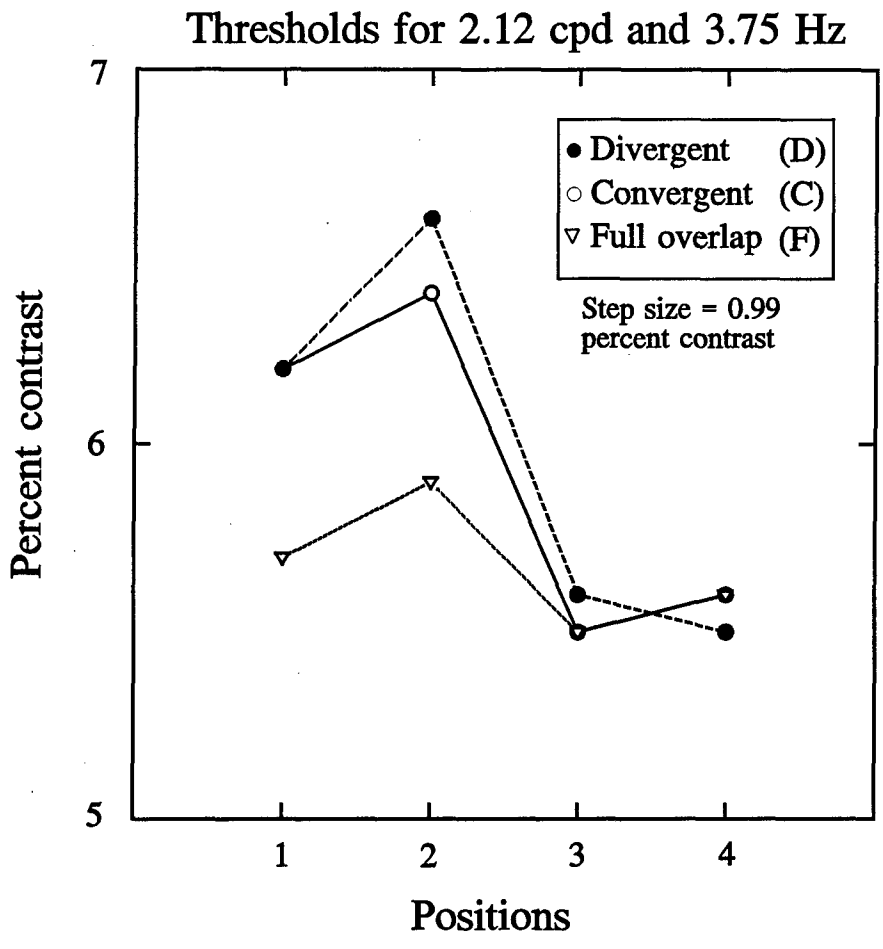

t - test	1	2	3	4
C<D	p=.112 f	p=.082	------	------
F<C	p<.001	p<.001	------	------
F<D	p<.001	p<.001	------	------
ANOVA	p<.001	p<.001	n.s.	n.s.

f = false

n.s.= not significant

Figure D6. *Thresholds for 2.12 cpd and 3.75 Hz. Means and standard errors of graphed data points are listed in Table C2. Bottom of figure shows results of statistical analyses from Table C6.*

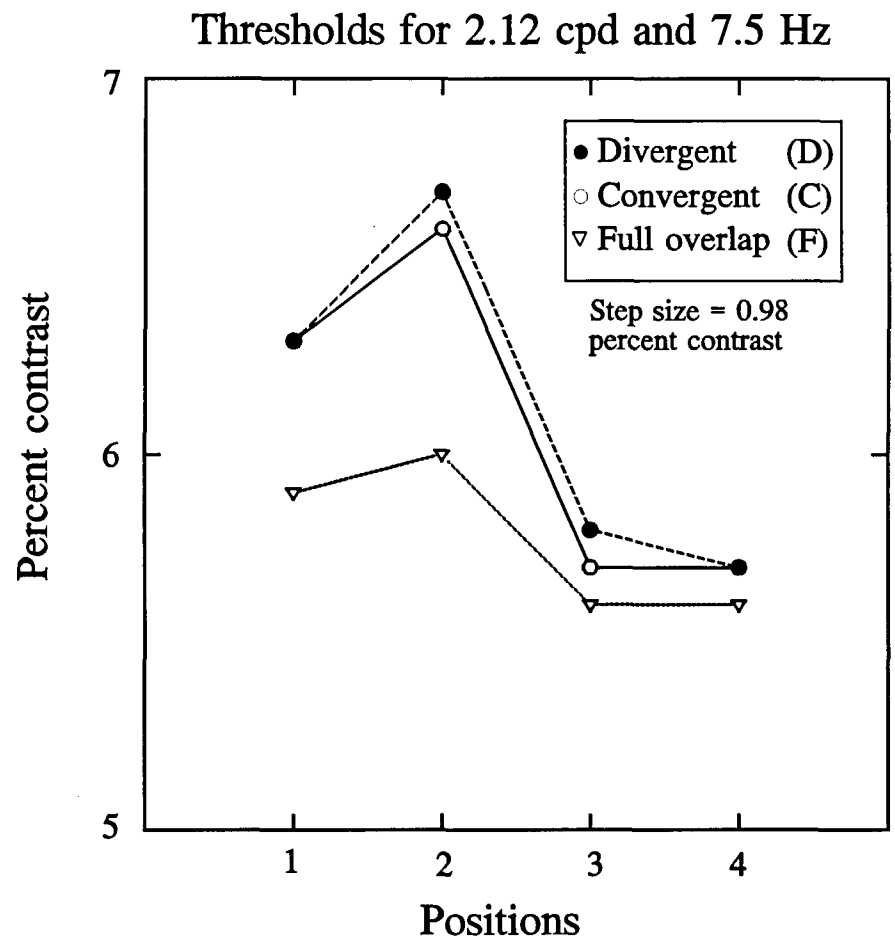

t - test	1	2	3	4
C<D	p=.338	p=.209	p=.151	------
F<C	p<.001	p<.001	p=.005	------
F<D	p<.001	p<.001	p<.001	------
ANOVA	p<.001	p<.001	p<.05	n.s.

n.s.= not significant

Figure D7. *Thresholds for 2.12 cpd and 7.5 Hz. Means and standard errors of graphed data points are listed in Table C2. Bottom of figure shows results of statistical analyses from Table C6.*

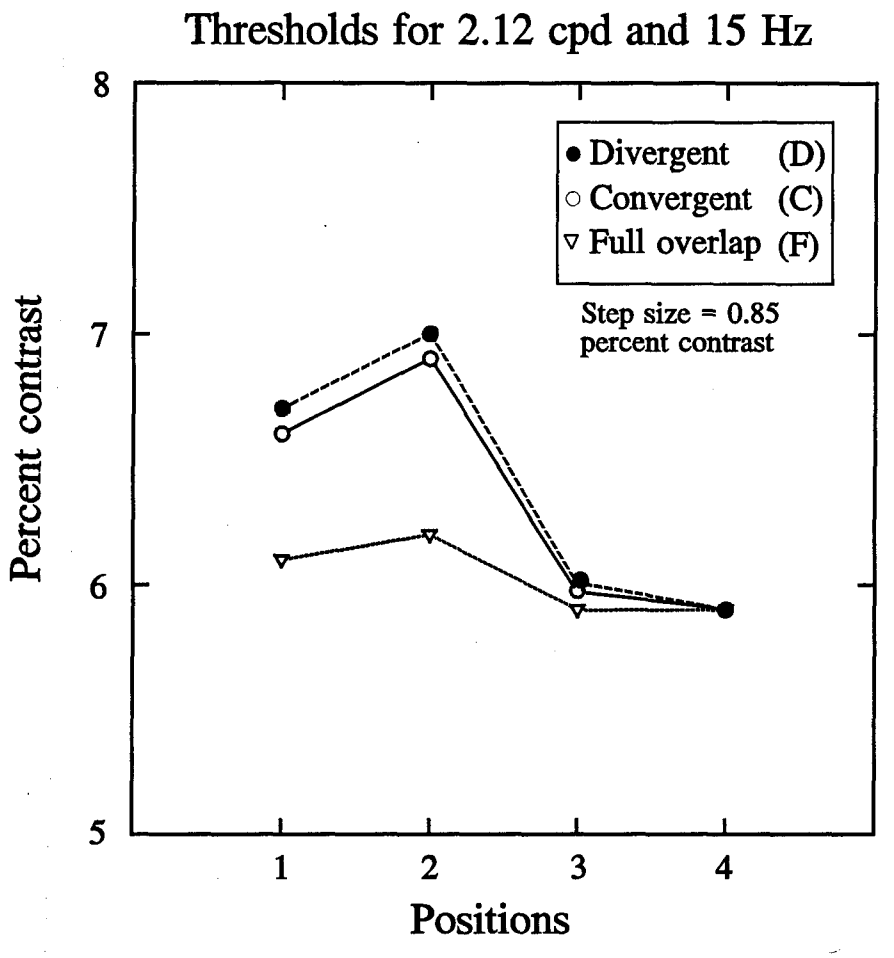

t - test	1	2	3	4
C<D	p=.431	p=.285	p=.078	------
F<C	p<.001	p<.001	p=.011	------
F<D	p<.001	p<.001	p=.003	------
ANOVA	p<.001	p<.001	p<.005	n.s.

n.s.= not significant

Figure D8. *Thresholds for 2.12 cpd and 15 Hz. Means and standard errors of graphed data points are listed in Table C2. Bottom of figure shows results of statistical analyses from Table C6.*

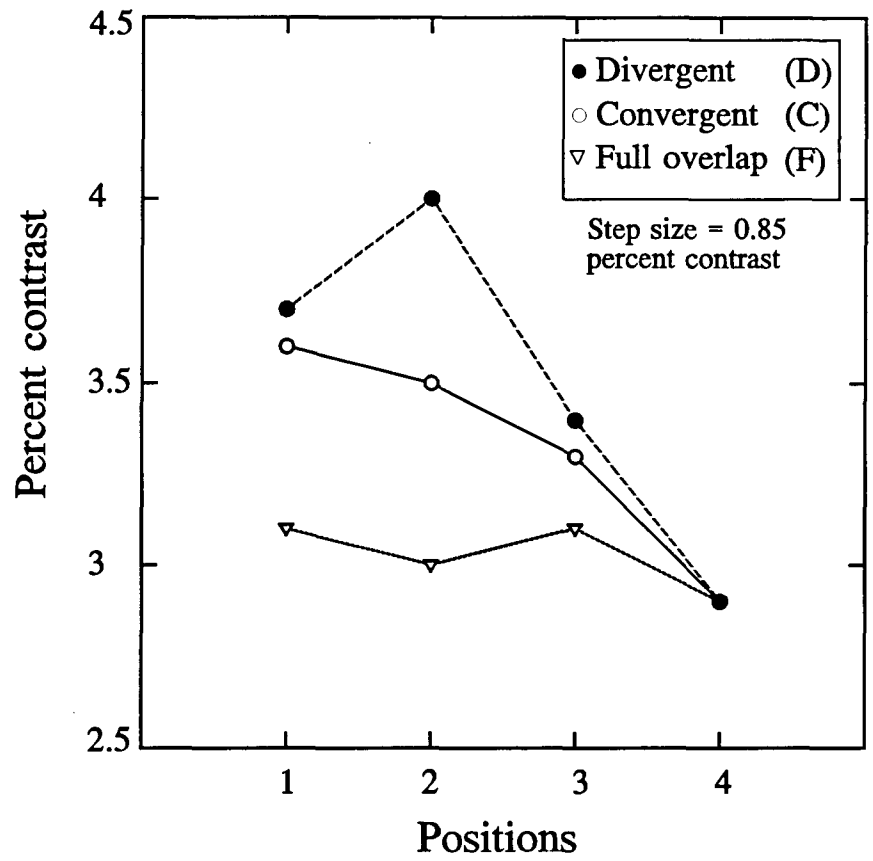

t - test	1	2	3	4
C<D	p=.404	p=.011	p=.294	------
F<C	p<.001	p<.001	p=.020	------
F<D	p<.001	p<.001	p=.006	------
ANOVA	p<.001	p<.001	p<.05	n.s.

n.s.= not significant

Figure D9. *Thresholds for 4.24 cpd and 0 Hz. Means and standard errors of graphed data points are listed in Table C3. Bottom of figure shows results of statistical analyses from Table C7.*

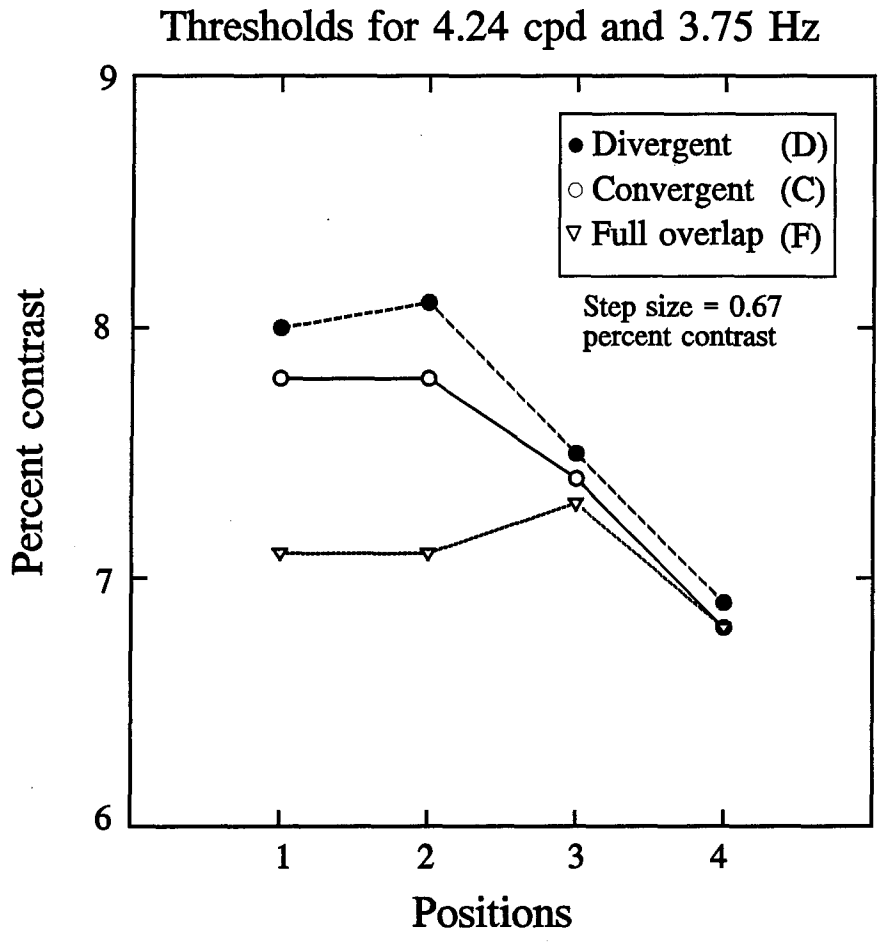

t - test	1	2	3	4
C<D	p=.162	p=.087	p=.038	------
F<C	p<.001	p<.001	p=.053	------
F<D	p<.001	p<.001	p<.001	------
ANOVA	p<.001	p<.001	p<.01	n.s.

n.s.= not significant

Figure D10. *Thresholds for 4.24 cpd and 3.75 Hz. Means and standard errors of graphed data points are listed in Table C3. Bottom of figure shows results of statistical analyses from Table C7.*

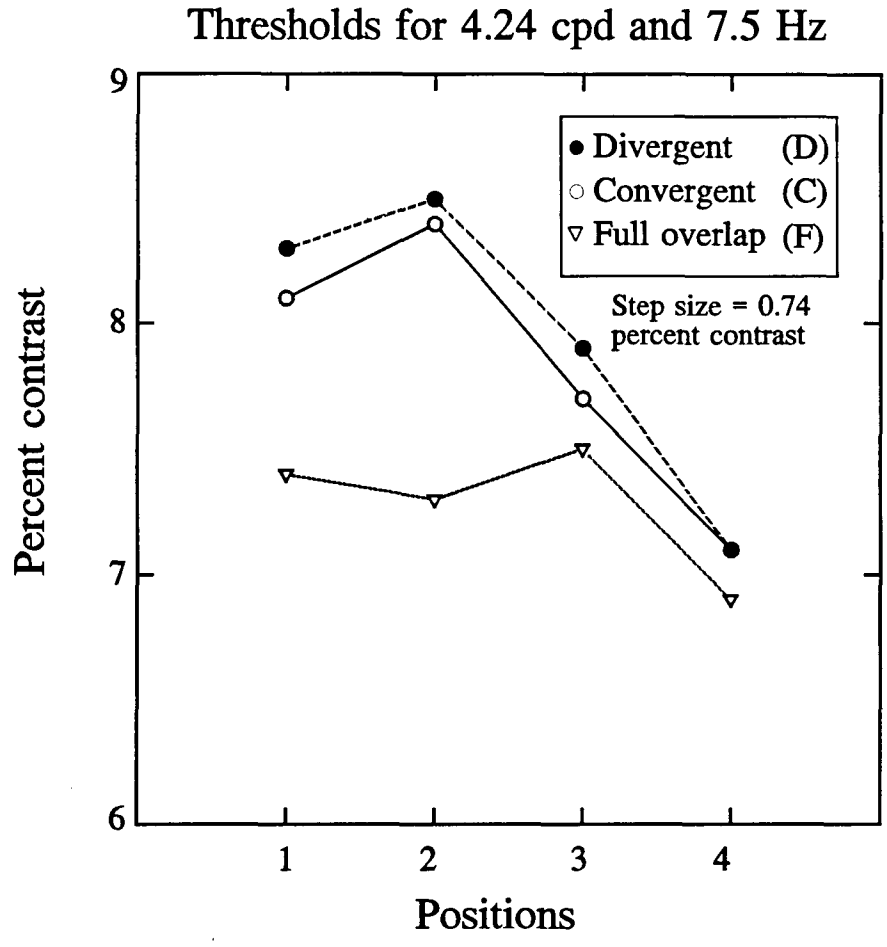

t - test	1	2	3	4
C<D	p=.202	p=.295	p=.024	------
F<C	p<.001	p<.001	p=.107	------
F<D	p<.001	p<.001	p=.007	------
ANOVA	p<.001	p<.001	p<.05	n.s.

n.s.= not significant

Figure D11. *Thresholds for 4.24 cpd and 7.5 Hz. Means and standard errors of graphed data points are listed in Table C3. Bottom of figure shows results of statistical analyses from Table C7.*

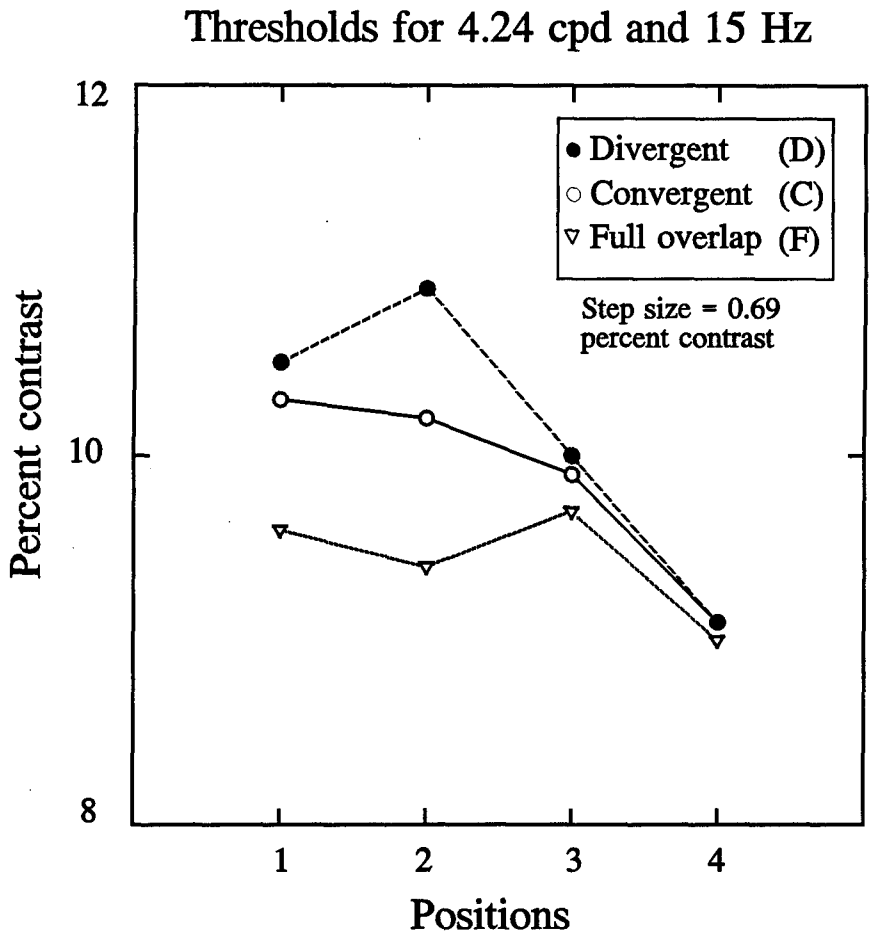

t - test	1	2	3	4
C<D	p=.197	p=.008	p=.441	------
F<C	p=.002	p<.001	p=.002	------
F<D	p<.001	p<.001	p=.010	------
ANOVA	p<.001	p<.001	p<.05	n.s.

n.s.= not significant

Figure D12. *Thresholds for 4.24 cpd and 15 Hz. Means and standard errors of graphed data points are listed in Table C3. Bottom of figure shows results of statistical analyses from Table C7.*

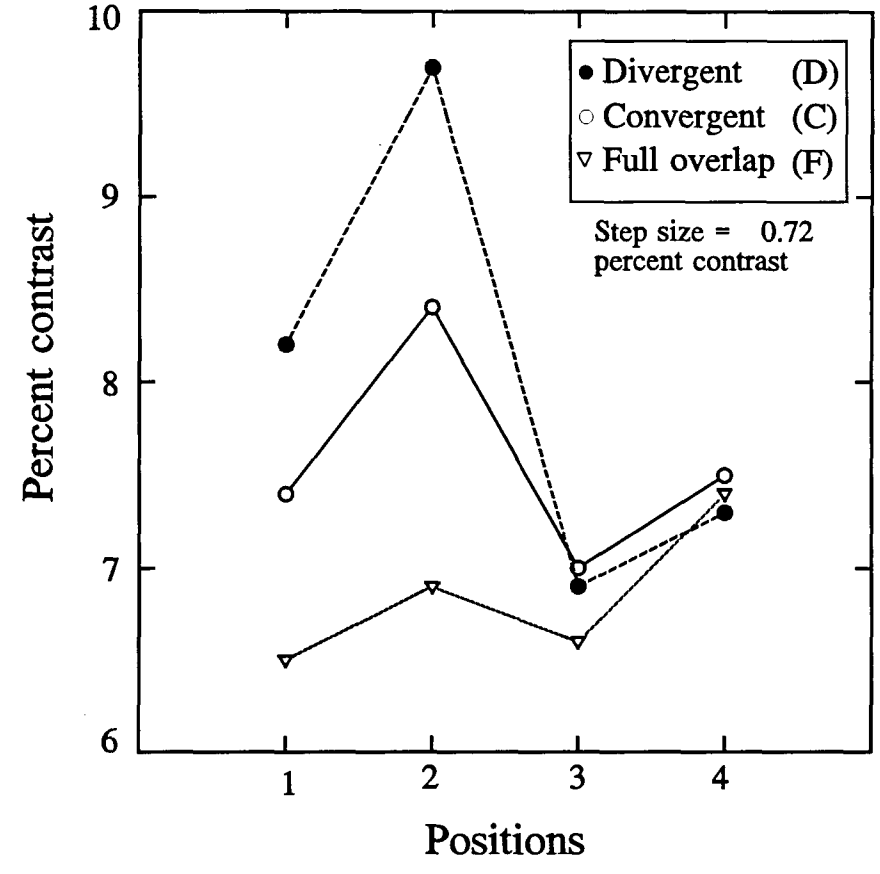

t - test	1	2	3	4
C<D	p=.027	p=.003	------	------
F<C	p=.007	p<.001	------	------
F<D	p<.001	p<.001	------	------
ANOVA	p<.001	p<.001	n.s.	n.s.

n.s.= not significant

Figure D13. *Thresholds for 8.48 cpd and 0 Hz. Means and standard errors of graphed data points are listed in Table C4. Bottom of figure shows results of statistical analyses from Table C8.*

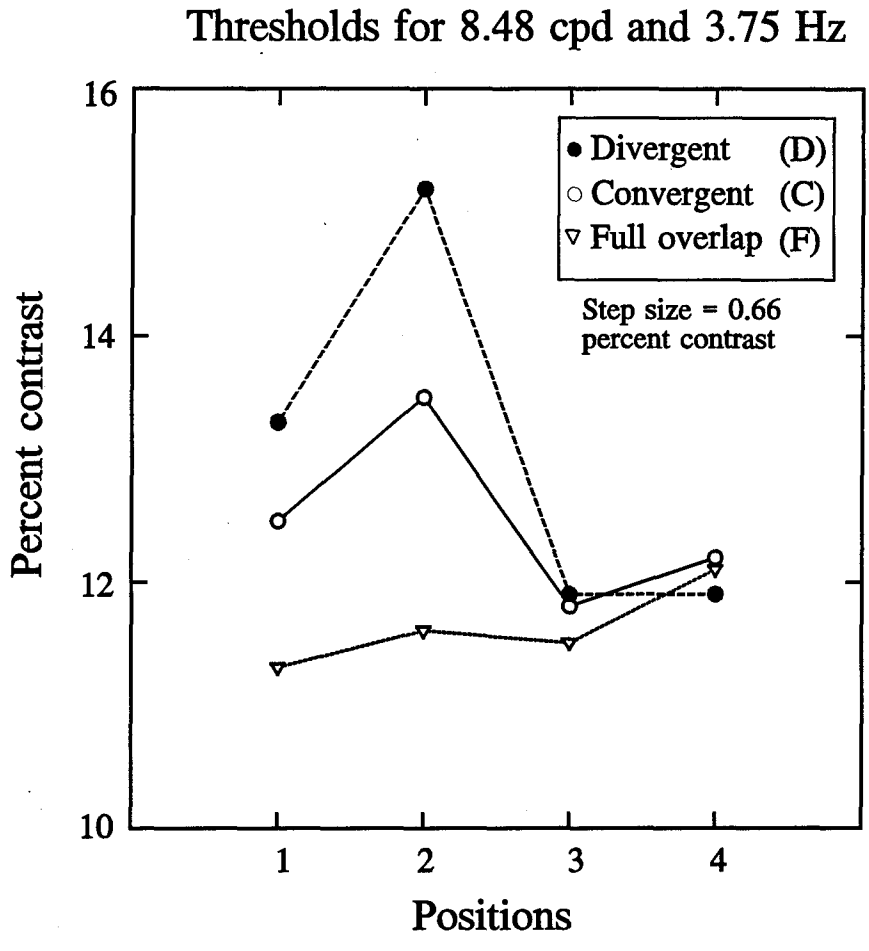

t - test	1	2	3	4
C<D	p=.043	p<.001	------	------
F<C	p=.004	p<.001	------	------
F<D	p<.001	p<.001	------	------
ANOVA	p<.001	p<.001	n.s.	n.s.

n.s.= not significant

Figure D14. *Thresholds for 8.48 cpd and 3.75 Hz. Means and standard errors of graphed data points are listed in Table C4. Bottom of figure shows results of statistical analyses from Table C8.*

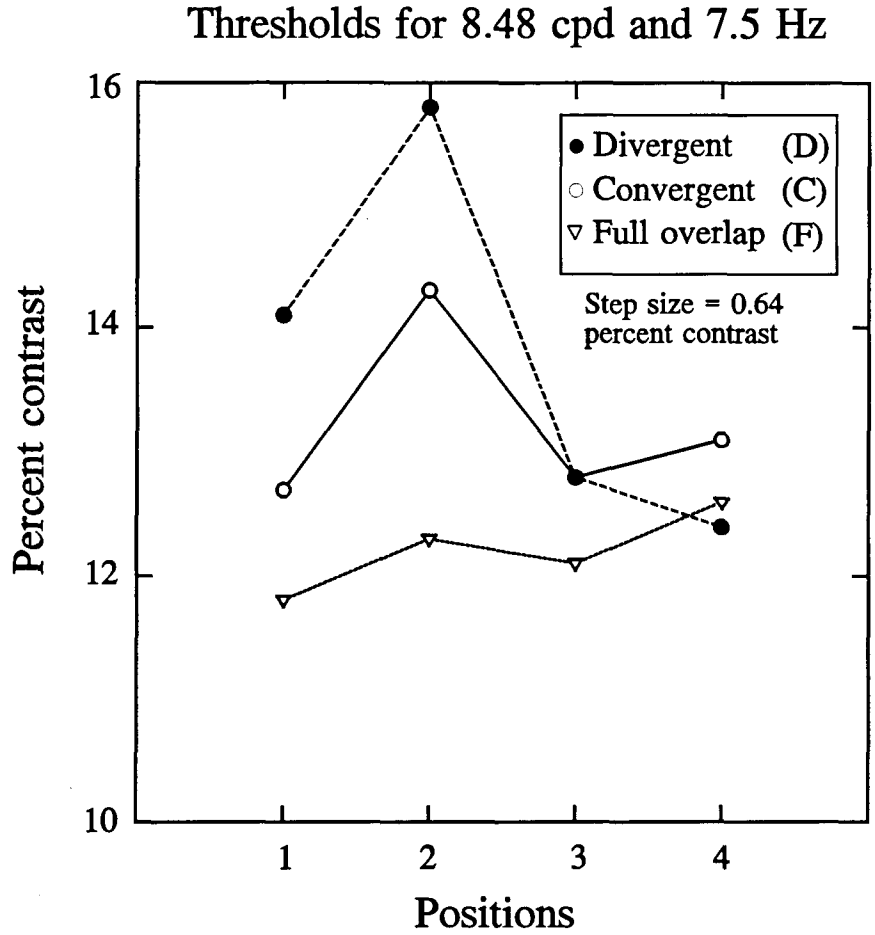

t - test	1	2	3	4
C<D	p=.008	p<.001	------	------
F<C	p=.030	p<.001	------	------
F<D	p<.001	p<.001	------	------
ANOVA	p<.001	p<.001	n.s.	n.s.

n.s.= not significant

Figure D15. *Thresholds for 8.48 cpd and 7.5 Hz. Means and standard errors of graphed data points are listed in Table C4. Bottom of figure shows results of statistical analyses from Table C8.*

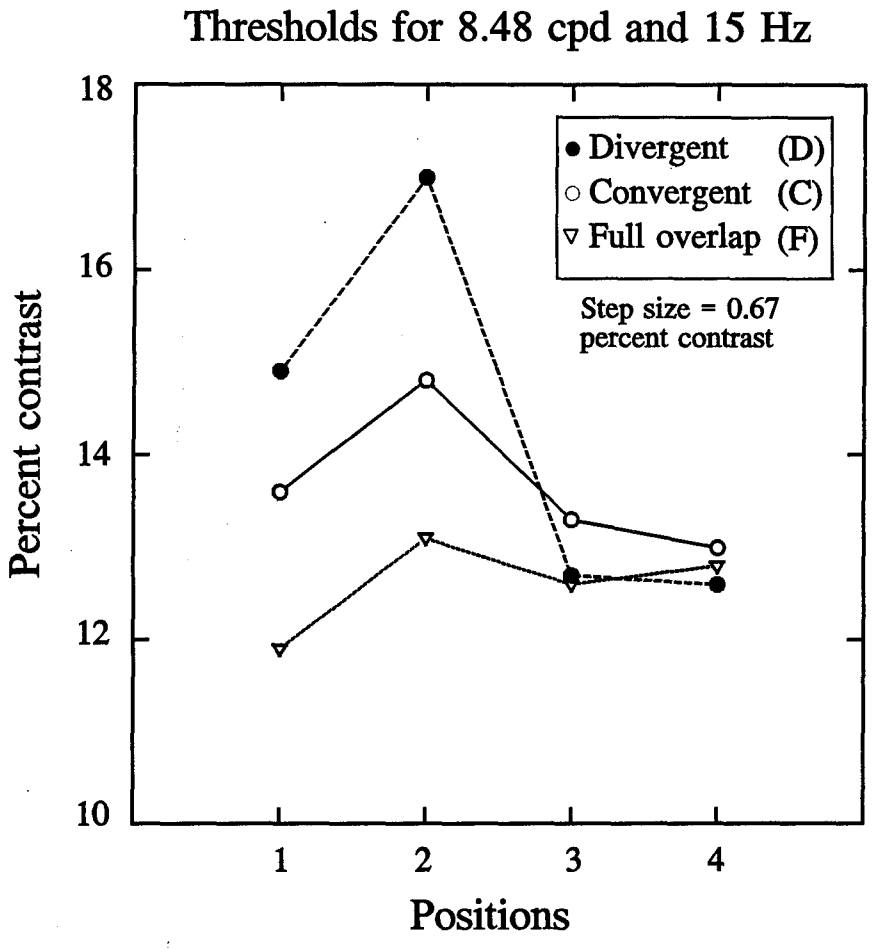

t - test	1	2	3	4
C<D	p=.011	p<.001	------	------
F<C	p=.005	p<.001	------	------
F<D	p<.001	p<.001	------	------
ANOVA	p<.001	p<.001	n.s.	n.s.

n.s.= not significant

Figure D16. *Thresholds for 8.48 cpd and 15 Hz. Means and standard errors of graphed data points are listed in Table C4. Bottom of figure shows results of statistical analyses from Table C8.*

Initial distribution

Commander, U.S. Army Natick Research, Development and Engineering Center
ATTN: SATNC-MIL (Documents Librarian)
Natick, MA 01760-5040

Chairman
National Transportation Safety Board
800 Independence Avenue, S.W.
Washington, DC 20594

Commander
10th Medical Laboratory
ATTN: Audiologist
APO New York 09180

Naval Air Development Center
Technical Information Division
Technical Support Detachment
Warminster, PA 18974

Commanding Officer, Naval Medical Research and Development Command
National Naval Medical Center
Bethesda, MD 20814-5044

Deputy Director, Defense Research and Engineering
ATTN: Military Assistant for Medical and Life Sciences
Washington, DC 20301-3080

Commander, U.S. Army Research Institute of Environmental Medicine
Natick, MA 01760

Library
Naval Submarine Medical Research Lab
Box 900, Naval Sub Base
Groton, CT 06349-5900

Executive Director, U.S. Army Human Research and Engineering Directorate
ATTN: Technical Library
Aberdeen Proving Ground, MD 21005

Commander
Man-Machine Integration System
Code 602
Naval Air Development Center
Warminster, PA 18974

Commander
Naval Air Development Center
ATTN: Code 602-B
Warminster, PA 18974

Commanding Officer
Armstrong Laboratory
Wright-Patterson
Air Force Base, OH 45433-6573

Director
Army Audiology and Speech Center
Walter Reed Army Medical Center
Washington, DC 20307-5001

Commander/Director
U.S. Army Combat Surveillance and Target Acquisition Lab
ATTN: SFAE-IEW-JS
Fort Monmouth, NJ 07703-5305

Director
Federal Aviation Administration
FAA Technical Center
Atlantic City, NJ 08405

Commander, U.S. Army Test
and Evaluation Command
Directorate for Test and Evaluation
ATTN: AMSTE-TA-M (Human Factors
Group)
Aberdeen Proving Ground,
MD 21005-5055

Naval Air Systems Command
Technical Air Library 950D
Room 278, Jefferson Plaza II
Department of the Navy
Washington, DC 20361

Director
U.S. Army Ballistic
Research Laboratory
ATTN: DRXBR-OD-ST Tech Reports
Aberdeen Proving Ground, MD 21005

Commander
U.S. Army Medical Research
Institute of Chemical Defense
ATTN: SGRD-UV-AO
Aberdeen Proving Ground,
MD 21010-5425

Commander
USAMRDALC
ATTN: SGRD-RMS
Fort Detrick, Frederick, MD 21702-5012

Director
Walter Reed Army Institute of Research
Washington, DC 20307-5100

HQ DA (DASG-PSP-O)
5109 Leesburg Pike
Falls Church, VA 22041-3258

Harry Diamond Laboratories
ATTN: Technical Information Branch
2800 Powder Mill Road
Adelphi, MD 20783-1197

U.S. Army Materiel Systems
Analysis Agency
ATTN: AMXSY-PA (Reports Processing)
Aberdeen Proving Ground
MD 21005-5071

U.S. Army Ordnance Center
and School Library
Simpson Hall, Building 3071
Aberdeen Proving Ground, MD 21005

U.S. Army Environmental
Hygiene Agency
ATTN: HSHB-MO-A
Aberdeen Proving Ground, MD 21010

Technical Library Chemical Research
and Development Center
Aberdeen Proving Ground, MD
21010-5423

Commander
U.S. Army Medical Research
Institute of Infectious Disease
ATTN: SGRD-UIZ-C
Fort Detrick, Frederick, MD 21702

Director, Biological
Sciences Division
Office of Naval Research
600 North Quincy Street
Arlington, VA 22217

Commandant
U.S. Army Aviation
Logistics School ATTN: ATSQ-TDN
Fort Eustis, VA 23604

Headquarters (ATMD)
U.S. Army Training
and Doctrine Command
ATTN: ATBO-M
Fort Monroe, VA 23651

IAF Liaison Officer for Safety
USAF Safety Agency/SEFF
9750 Avenue G, SE
Kirtland Air Force Base
NM 87117-5671

Naval Aerospace Medical
Institute Library
Building 1953, Code 03L
Pensacola, FL 32508-5600

Command Surgeon
HQ USCENTCOM (CCSG)
U.S. Central Command
MacDill Air Force Base, FL 33608

Director
Directorate of Combat Developments
ATTN: ATZQ-CD
Building 515
Fort Rucker, AL 36362

U.S. Air Force Institute
of Technology (AFIT/LDEE)
Building 640, Area B
Wright-Patterson
Air Force Base, OH 45433

Henry L. Taylor
Director, Institute of Aviation
University of Illinois-Willard Airport
Savoy, IL 61874

Chief, National Guard Bureau
ATTN: NGB-ARS
Arlington Hall Station
111 South George Mason Drive
Arlington, VA 22204-1382

Commander
U.S. Army Aviation and Troop Command
ATTN: AMSAT-R-ES
4300 Goodfellow Bouvelard
St. Louis, MO 63120-1798

U.S. Army Aviation and Troop Command
Library and Information Center Branch
ATTN: AMSAV-DIL
4300 Goodfellow Boulevard
St. Louis, MO 63120

Federal Aviation Administration
Civil Aeromedical Institute
Library AAM-400A
P.O. Box 25082
Oklahoma City, OK 73125

Commander
U.S. Army Medical Department
and School
ATTN: Library
Fort Sam Houston, TX 78234

Commander
U.S. Army Institute of Surgical Research
ATTN: SGRD-USM
Fort Sam Houston, TX 78234-6200

AAMRL/HEX
Wright-Patterson
Air Force Base, OH 45433

Air Unoiversity Library
(AUL/LSE)
Maxwell Air Force Base, AL 36112

Product Manager
Aviation Life Support Equipment
ATTN: SFAE-AV-LSE
4300 Goodfellow Boulevard
St. Louis, MO 63120-1798

Commander and Director
USAE Waterways Experiment Station
ATTN: CEWES-IM-MI-R,
CD Department
3909 Halls Ferry Road
Vicksburg, MS 39180-6199

Commanding Officer
Naval Biodynamics Laboratory
P.O. Box 24907
New Orleans, LA 70189-0407

Assistant Commandant
U.S. Army Field Artillery School
ATTN: Morris Swott Technical Library
Fort Sill, OK 73503-0312

Mr. Peter Seib
Human Engineering Crew Station
Box 266
Westland Helicopters Limited
Yeovil, Somerset BA20 2YB UK

U.S. Army Dugway Proving Ground
Technical Library, Building 5330
Dugway, UT 84022

U.S. Army Yuma Proving Ground
Technical Library
Yuma, AZ 85364

AFFTC Technical Library
6510 TW/TSTL
Edwards Air Force Base,
CA 93523-5000

Commander
Code 3431
Naval Weapons Center
China Lake, CA 93555

Aeromechanics Laboratory
U.S. Army Research and Technical Labs
Ames Research Center, M/S 215-1
Moffett Field, CA 94035

Sixth U.S. Army
ATTN: SMA
Presidio of San Francisco, CA 94129

Commander
U.S. Army Aeromedical Center
Fort Rucker, AL 36362

Strughold Aeromedical Library
Document Service Section
2511 Kennedy Circle
Brooks Air Force Base, TX 78235-5122

Dr. Diane Damos
Department of Human Factors
ISSM, USC
Los Angeles, CA 90089-0021

U.S. Army White Sands
Missile Range
ATTN: STEWS-IM-ST
White Sands Missile Range, NM 88002

U.S. Army Aviation Engineering
Flight Activity
ATTN: SAVTE-M (Tech Lib) Stop 217
Edwards Air Force Base, CA 93523-5000

Ms. Sandra G. Hart
Ames Research Center
MS 262-3
Moffett Field, CA 94035

Commander
USAMRDALC
ATTN: SGRD-UMZ
Fort Detrick, Frederick, MD 21702-5009

Commander
U.S. Army Health Services Command
ATTN: HSOP-SO
Fort Sam Houston, TX 78234-6000

U. S. Army Research Institute
Aviation R&D Activity
ATTN: PERI-IR
Fort Rucker, AL 36362

Commander
U.S. Army Safety Center
Fort Rucker, AL 36362

U.S. Army Aircraft Development
Test Activity
ATTN: STEBG-MP-P
Cairns Army Air Field
Fort Rucker, AL 36362

Commander
USAMRDALC
ATTN: SGRD-PLC (COL R. Gifford)
Fort Detrick, Frederick, MD 21702

TRADOC Aviation LO
Unit 21551, Box A-209-A
APO AE 09777

Netherlands Army Liaison Office
Building 602
Fort Rucker, AL 36362

British Army Liaison Office
Building 602
Fort Rucker, AL 36362

Italian Army Liaison Office
Building 602
Fort Rucker, AL 36362

Directorate of Training Development
Building 502
Fort Rucker, AL 36362

Chief
USAHEL/USAAVNC Field Office
P. O. Box 716
Fort Rucker, AL 36362-5349

Commander, U.S. Army Aviation Center
and Fort Rucker
ATTN: ATZQ-CG
Fort Rucker, AL 36362

Chief
Test & Evaluation Coordinating Board
Cairns Army Air Field
Fort Rucker, AL 36362

Canadian Army Liaison Office
Building 602
Fort Rucker, AL 36362

German Army Liaison Office
Building 602
Fort Rucker, AL 36362

French Army Liaison Office
USAAVNC (Building 602)
Fort Rucker, AL 36362-5021

Australian Army Liaison Office
Building 602
Fort Rucker, AL 36362

Dr. Garrison Rapmund
6 Burning Tree Court
Bethesda, MD 20817

Commandant, Royal Air Force
Institute of Aviation Medicine
Farnborough, Hampshire GU14 6SZ UK

Defense Technical Information
Cameron Station, Building 5
Alexandra, VA 22304-6145

Commander, U.S. Army Foreign Science
and Technology Center
AIFRTA (Davis)
220 7th Street, NE
Charlottesville, VA 22901-5396

Commander
Applied Technology Laboratory
USARTL-ATCOM
ATTN: Library, Building 401
Fort Eustis, VA 23604

Commander, U.S. Air Force
Development Test Center
101 West D Avenue, Suite 117
Eglin Air Force Base, FL 32542-5495

Aviation Medicine Clinic
TMC #22, SAAF
Fort Bragg, NC 28305

Dr. H. Dix Christensen
Bio-Medical Science Building, Room 753
Post Office Box 26901
Oklahoma City, OK 73190

Commander, U.S. Army Missile
Command
Redstone Scientific Information Center
ATTN: AMSMI-RD-CS-R
/ILL Documents
Redstone Arsenal, AL 35898

Director
Army Personnel Research Establishment
Farnborough, Hants GU14 6SZ UK

U.S. Army Research and Technology
Laboratories (AVSCOM)
Propulsion Laboratory MS 302-2
NASA Lewis Research Center
Cleveland, OH 44135

Commander
USAMRDALC
ATTN: SGRD-ZC (COL John F. Glenn)
Fort Detrick, Frederick, MD 21702-5012

Dr. Eugene S. Channing
166 Baughman's Lane
Frederick, MD 21702-4083

U.S. Army Medical Department
and School
USAMRDALC Liaison
ATTN: HSMC-FR
Fort Sam Houston, TX 78234

Dr. A. Kornfield
895 Head Street
San Francisco, CA 94132-2813

NVESD
AMSEL-RD-NV-ASID-PST
(Attn: Trang Bui)
10221 Burbeck Road
Fort Belvior, VA 22060-5806

CA Av Med
HQ DAAC
Middle Wallop
Stockbridge, Hants S020 8DY UK

Dr. Christine Schlichting
Behavioral Sciences Department
Box 900, NAVUBASE NLON
Groton, CT 06349-5900

Commander, HQ AAC/SGPA
Aerospace Medicine Branch
162 Dodd Boulevard, Suite 100
Langley Air Force Base,
VA 23665-1995

Commander
Aviation Applied Technology Directorate
ATTN: AMSAT-R-TV
Fort Eustis, VA 23604-5577

COL Yehezkel G. Caine, MD
Surgeon General, Israel Air Force
Aeromedical Center Library
P. O. Box 02166 I.D.F.
Israel

Director
Aviation Research, Development
and Engineering Center
ATTN: AMSAT-R-Z
4300 Goodfellow Boulevard
St. Louis, MO 63120-1798

Commander
USAMRDALC
ATTN: SGRD-ZB (COL C. Fred Tyner)
Fort Detrick, Frederick, MD 21702-5012